# 7 SCIENTIFIC HIGHLIGHT OF THE MONTH: "Short-range correlations in disordered systems: the Non-local Coherent-Potential Approximation"

---

## Short-range correlations in disordered systems: the nonlocal coherent-potential aproximation

D. A. Rowlands

*H.H. Wills Physics Laboratory, University of Bristol, Bristol BS8 1TL, U.K.*

**Abstract**

A review of the nonlocal coherent-potential approximation (NLCPA) is presented for describing short-range correlations in substitutionally-disordered systems. Originally introduced by Jarrell and Krishnamurthy to generalise the widely used coherent-potential approximation (CPA) approach in the context of a tight-binding model, the NLCPA has since been implemented within KKR multiple scattering theory (KKR-NLCPA) and combined with density functional theory for *ab-initio* calculations (self-consistent-field (SCF)-KKR-NLCPA). Here an application to the $Cu_{50}Zn_{50}$ disordered alloy is described, demonstrating the role of charge transfer and the variation of the total energy as a function of chemical short-range order. Significantly, the method will enable important problems involving systems with spin, strain, or valency fluctuations to be tackled in a parameter-independent and material-specific way.

## 1 Introduction

In substitutionally-disordered systems such as the solid solution phase of an alloy, we are interested in configurationally-averaged properties. For example, for a binary solid solution we should in principle calculate properties for each of the $2^N$ possible configuations (where $N$ is the number of sites in the lattice) and then take a statistical average according to the probability of each configuration occuring. Clearly this is a computationally impossible task and so some approximation scheme is needed. For many years the coherent-potential approximation (CPA) [1], a mean-field approach, has been widely used to deal with such an ensemble of disorder configurations. Its application within the multiple-scattering Korringa-Kohn-Rostoker [2, 3] (KKR) electronic structure method has been particularly successful. Indeed, the KKR-CPA [4, 5] and its LMTO derivatives are the only electronic structure methods which can deal with disordered systems and be combined with density functional theory (DFT) [6, 7] for *ab-initio* calculations. Such self-consistent-field (SCF)-KKR-CPA [8–11] calculations require, say for a binary solid solution, the self-consistent determination of two 'partially-averaged' single-site charge densities

$\overline{\rho}_A$ and $\overline{\rho}_B$ only, where the CPA treats the configurational averages over all possible chemical environments as a mean field. As well as application to a wide range of disordered alloys, the SCF-KKR-CPA has also been adapted to deal with the 'disordered local moment' spin fluctuations in itinerant magnets at finite temperature [12, 13]. However, despite numerous successes, the SCF-KKR-CPA has a serious limitation due to the single-site mean-field nature of the CPA itself, specifically it neglects correlations in the occupation of the lattice sites. It is therefore unable to include important short-range environmental effects present in the individual configurations into its configurationally-averaged description of the system. These include 1. chemical short-range order (SRO) i.e. the tendency for sites to either be surrounded by like sites (clustering) or by unlike sites (ordering) on short length scales, 2. charge correlations in alloys i.e. the Madelung contribution to the total energy, 3. lattice displacements in alloys i.e. deviations from the average rigid lattice due to size mis-match between the constituent atoms, and 4. correlations in the orientations of the local moments in metallic magnets at finite temperature.

The development of a satisfactory multi-site or cluster generalisation of the CPA in order to address this missing physics has remained a long-standing problem [14]. However, a recent theory, the nonlocal coherent potential approximation (NLCPA) [15], appears to possess all the attributes required for a satisfactory generalisation of the CPA. It was originally introduced by Jarrell and Krishnamurthy [15] in the context of a tight-binding model Hamiltonian as the static version of the dynamical cluster approximation (DCA) [16, 17] used for describing short-range dynamical correlations in the Hubbard model. The NLCPA was subsequently derived within the KKR framework [18], and the first KKR-NLCPA [18, 19] implementation for a realistic system was given in [20]. Moreover, the KKR-NLCPA has recently been combined with DFT and, significantly, the resulting SCF-KKR-NLCPA [21] method enables the total energy to be investigated as a function of chemical SRO. As a generalisation of the conventional SCF-KKR-CPA, it requires the self-consistent determination of a set of 'partially-averaged' cluster charge densities $\{\overline{\underline{\rho}}_\gamma\}$ where the NLCPA treats the configurational averages over all possible chemical environments as a mean field. Since possible charge transfer between the cluster sites can now be explicitly accounted for, the missing charge-correlation (Madelung) [22–25] electrostatic contribution to the total energy can be systematically taken into account as the cluster size increases. In addition to alloys, further important future developments include application to systems with spin fluctuations as mentioned above, and pseudo-alloy problems such as valency fluctuations [26].

Before summarising the contents of this highlight, it is worth mentioning some of the advantageous properties of the NLCPA which facilitates its application to the above problems. A key advantage of the NLCPA is that, like the conventional CPA, it preserves the full translational and point-group symmetry of the underlying lattice. This means the NLCPA is computationally feasible for realistic systems since the reciprocal-space Brillouin zone (BZ) integration does not scale as the cluster size increases like it would for say a supercell calculation. This feature also means the NLCPA can be used to investigate nonlocal disorder effects on Fermi surfaces [27] and transport properties e.g. resistivity in K-state alloys [28]. Another advantage of the NLCPA is that it is a self-consistent theory and is therefore able to give a self-consistent treatment of chemical SRO. This also means significant nonlocal effects such as large fractions of the Madelung energy in alloys can be captured using only small clusters, as will be shown later.

A brief outline of this highlight now follows. In order to explain the idea of the NLCPA as explicitly as possible, Section 2 first introduces the NLCPA in the context of a simple tight-binding model Hamiltonian. This enables a description of nonlocal correlations in the context of the disorder problem to be

given in terms of the familiar Dyson equation involving the self-energy. The idea of the NLCPA as a systematic method for including these correlations is described and the computational algorithm of the method, which greatly aids an understanding of the formalism, is also detailed. Following this, a numerical investigation of the NLCPA is presented for a simple one-dimensional model in order to examine the validity of the method. In Section 3, following a brief introduction to KKR multiple scattering theory and a brief overview of the conventional SCF-KKR-CPA, the basic KKR-NLCPA formalism is outlined by making analogy with the tight-binding formalism of Section 2 where possible. The formalism presented here assumes the potentials have already been self-consistently determined using the SCF-KKR-CPA, so the calculations presented are 'first-pass' only in the sense that charge self-consistency with respect to the KKR-NLCPA medium itself is not enforced. Section 4 details the full charge self-consistent (SCF)-KKR-NLCPA formalism, including the expression for the total energy and a description of the charge-correlation (Madelung) term. An application to the $Cu_{50}Zn_{50}$ system is described, demonstrating the role of charge transfer and the variation of the total energy as a function of chemical SRO. Finally, conclusions are made and possible future work discussed in Section 5.

## 2 Tight-binding NLCPA

**Nonlocal correlations**

Consider a general tight-binding model Hamiltonian

$$H^{ij} = \epsilon^i \delta_{ij} + W^{ij}(1 - \delta_{ij}) \tag{1}$$

for a binary alloy defined by a hopping amplitude $W^{ij}$ and site energies $\epsilon_A$ and $\epsilon_B$. In terms of the site occupation numbers $\xi_i$ which take on values of 0 and 1 depending on whether the site is occupied by an $A$-atom or a $B$-atom, the usual Green's function $G^{ij}(E)$ describing the propagation of an electron in the lattice satisfies the Dyson equation

$$G^{ij} = G_0^{ij} + \sum_k G_0^{ik} \epsilon^k G^{kj} \tag{2}$$

where $\epsilon_i = \xi_i \epsilon_A + (1 - \xi_i)\epsilon_B$ and $G_0$ is the free-particle Green's function. We are interested in $\left\langle G^{ij} \right\rangle$, the average of $G^{ij}$ over all possible sets of disorder configurations $\{\xi\}$. By expanding (2) and averaging term by term, it is possible to express $\left\langle G^{ij} \right\rangle$ in the form

$$\left\langle G^{ij} \right\rangle = G_0^{ij} + \sum_{p,q} G_0^{ip} \Sigma^{pq} \left\langle G^{qj} \right\rangle \tag{3}$$

where $\Sigma^{ij}$ is the exact self-energy. Here $\Sigma^{ij}$ is a static nonlocal quantity associated with a configurational average over the disorder configurations. It is important to give a physical interpretation of (3). Since (3) is in the form of a Dyson equation, it may be interpreted as describing an electron propagating through an *effective medium* in which the site-diagonal part of $\Sigma^{ij}$ decribes an effective on-site energy, and the site off-diagonal part describes an effective correction to the hopping. Significantly, since $\left\langle G^{ij} \right\rangle$ and correspondingly $\Sigma^{ij}$ both possess the full translational symmetry of the underlying lattice, (3) may be expressed in reciprocal space as

$$\langle G(\mathbf{k}) \rangle = G_0(\mathbf{k}) + G_0(\mathbf{k})\Sigma(\mathbf{k}) \langle G(\mathbf{k}) \rangle = (E - W(\mathbf{k}) - \Sigma(\mathbf{k}))^{-1} \tag{4}$$

Then $\langle G^{ij} \rangle$ may be calculated via the BZ integral

$$\langle G^{ij} \rangle = \frac{1}{\Omega_{BZ}} \int_{\Omega_{BZ}} (E - W(\mathbf{k}) - \Sigma(\mathbf{k}))^{-1} \, e^{i\mathbf{k}(\mathbf{R}_i - \mathbf{R}_j)} \tag{5}$$

from which observable properties can be calculated. In practice it is of course unfeasible to average over all possible configurations of an infinite (or very large) lattice. The aim of an effective medium theory is therefore to determine an approximation to the exact self-energy $\Sigma^{ij}$ and corresponding $\langle G^{ij} \rangle$. The well-known CPA approach is to map the problem to that of a self-consistent single-site (local) impurity problem where one is only required to explicitly average over the possible configurations of a single site. The limitation of this approach is that all nonlocal physics is treated at mean-field level only. In other words, a site only feels the average effect of its environment and so nonlocal correlations in the disorder configurations are neglected. Therefore the CPA self-energy is a single-site quantity $\Sigma^{ii}$ and has no dependence on momentum $\mathbf{k}$. A brief overview of the CPA now follows.

**Conventional CPA**

As mentioned above, the main approximation made by the CPA [1] is to assume a site-diagonal translationally-invariant self-energy $\Sigma^{ii}\delta_{ij}$. The CPA effective medium is then described by the equation

$$\overline{G}^{ij} = G_0^{ij} + \sum_k G_0^{ik} \Sigma^{kk} \overline{G}^{kj} \tag{6}$$

In order to determine the medium, let us consider any site $i$. By removing the sum over all sites $k$ and making up for the neglected terms by replacing the free particle Green's function with the cavity Green's function $\mathcal{G}^{ii}$, the site-diagonal part of (6) at site $i$ can be formally rewritten in the form

$$\overline{G}^{ii} = \mathcal{G}^{ii} + \mathcal{G}^{ii} \, \Sigma^{ii} \, \overline{G}^{ii} = \left( \left( \mathcal{G}^{ii} \right)^{-1} - \Sigma^{ii} \right)^{-1} \tag{7}$$

where $\mathcal{G}^{ii}$ can be written in terms of an expansion over the remaining lattice sites. It can be seen that $\mathcal{G}^{ii}$ depends only on the medium surrounding site $i$ and is independent of the chemical occupation of $i$ itself. It is therefore straightforward to define the Green's function for a real *impurity* embedded in the medium simply by replacing the effective site energy $\Sigma^{ii}$ with a real site energy $\epsilon_\alpha^i$ at site $i$, where $\alpha = A$ or $B$. From (7) this is given by

$$G_\alpha^{ii} = \left( \left( \mathcal{G}^{ii} \right)^{-1} - \epsilon_\alpha^i \right)^{-1} = \left( \Sigma^{ii} - \epsilon_\alpha^i + (\overline{G}^{ii})^{-1} \right)^{-1} \tag{8}$$

Now the CPA demands that

$$\sum_\alpha P_\alpha G_\alpha^{ii} = \overline{G}^{ii} \tag{9}$$

where $P_\alpha$ is the probability that site $i$ is of chemical type $\alpha$. In other words, the replacement of an effective site energy by a real site energy should, on the average, produce no change to the CPA medium. Since the medium is translationally-invariant, it follows from (6) that $\overline{G}^{ii}$ must also satisfy the BZ integral

$$\overline{G}^{ii} = \frac{1}{\Omega_{BZ}} \int_{\Omega_{BZ}} d\mathbf{k} \, \left( E - \Sigma^{(ii)} - W(\mathbf{k}) \right)^{-1} \tag{10}$$

The CPA medium is therefore determined from a self-consistent solution of (9) and (10).

**Idea of the NLCPA**

In order to go beyond the CPA and include nonlocal correlations in the disorder configurations, it is clear that we need to generalise the single-site CPA approach and average over an ensemble of impurity *cluster* configurations. This would enable us to define a cluster self-energy $\Sigma^{IJ}$, where $\{I, J\}$ are cluster sites. In brief, knowledge of correlated hoppings for specific cluster disorder configurations means the intra-cluster hopping would be modified on the average and therefore the self-energy would gain an off-diagonal part. Although such a generalisation appears straightforward, the main difficulty is in preserving translational invariance and formulating a consistent treatment in reciprocal space, for example treating a site at say the boundary of the cluster in an identical manner as say a site at the centre of the cluster. The NLCPA solves the problem of maintaining translational invariance by *imposing Born-von Karman boundary conditions on the cluster*. The idea is to self-consistently embed a cluster (or finite-sized lattice) with Born-von Karman boundary conditions into an infinite lattice with Born-von Karman boundary conditions. The extent of nonlocal correlations included in the resulting effective medium are limited by the size of the cluster, however all symmetries of the underlying lattice are preserved.

**Cluster with Born-von Karman boundary conditions**

The first step in the derivation of the NLCPA is to solve the problem of a cluster with Born-von Karman (periodic) boundary conditions. This essentially means reducing the size of a conventional lattice with Born-von Karman boundary conditions to contain only a cluster of $N_c$ sites, so that the edges of the cluster map round to the other end along each axis. Since the lattice constant is unchanged, the boundaries of the BZ will remain the same, however it will now contain only $N_c$ evenly spaced $\mathbf{k}$ points referred to as the set of *cluster momenta* $\{\mathbf{K}_n\}$ [15], where $n = 1, .., N_c$. Therefore the conventional lattice Fourier transform used in the $N_c \to \infty$ limit reduces to the cluster Fourier transform

$$\frac{1}{N_c} \sum_{\mathbf{K}_n} e^{i\mathbf{K}_n(\mathbf{R}_I - \mathbf{R}_J)} = \delta_{IJ} \tag{11}$$

which relates the real-space cluster sites $\{I\}$ (denoted by capital letters) to the corresponding set of cluster momenta $\{\mathbf{K}_n\}$ [15]. Significantly, averaged cluster quantities are now translationally-invariant and can be related in real and reciprocal space through (11), for example for the cluster self-energy we have

$$\Sigma_{cl}^{IJ} = \frac{1}{N_c} \sum_{\mathbf{K}_n} \Sigma_{cl}(\mathbf{K}_n) e^{i\mathbf{K}_n(\mathbf{R}_I - \mathbf{R}_J)} \quad \text{and} \quad \Sigma_{cl}(\mathbf{K}_n) = \sum_J \Sigma_{cl}^{IJ} e^{-i\mathbf{K}_n(\mathbf{R}_I - \mathbf{R}_J)} \tag{12}$$

However, there are restrictions on the possible choices of cluster that may be used when mapping the cluster to the lattice. As explained in Ref. [15], it must be possible to surround the cluster sites with a space-filling tile, the principal axes of which must point along a high symmetry direction of the underlying lattice. An example cluster and tile for a square lattice in 2D with $N_c = 4$ is shown in Fig. 1(a). Note that in a supercell calculation, this real space tile would correspond to a reciprocal space tile centred at one of the points $\{\mathbf{K}_n\}$, which would be the new (smaller) BZ. However, the NLCPA is not a supercell calculation and the idea is to use $N_c$ such tiles centred at each of the cluster momenta $\{\mathbf{K}_n\}$ to fill out the original BZ of the underlying lattice, thus preserving translational invariance. This is shown for the same example as above in Fig. 1(b). Importantly, the shape and size of the real space tile surrounding the cluster sites corresponds to the shape and size of the reciprocal space tiles surrounding the cluster momenta.

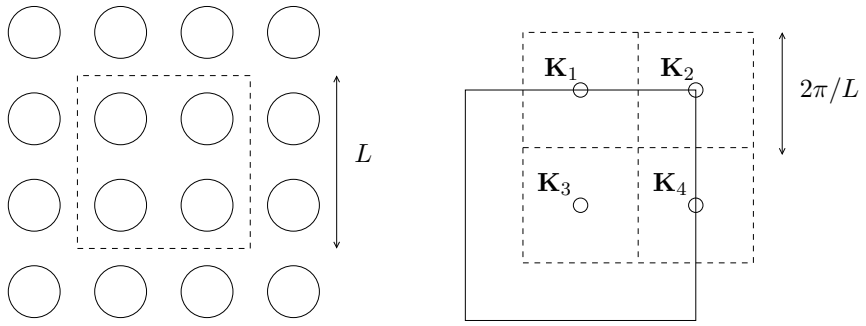


Figure 1: (a) Real-space tile for a 2D square lattice with cluster size $N_c = 4$. The linear length of the tile is $L = 2a$ where $a$ is the lattice constant. (b) Corresponding reciprocal-space tiles centred at the (periodic) cluster momenta $\{\mathbf{K}_n\}$. The solid line denotes the 1st BZ. Note that parts of tiles lying outside the 1st BZ can be translated through reciprocal lattice vectors to lie inside the 1st BZ.

**Mapping cluster to lattice**

In order to self-consistently determine the medium, we first need to map the cluster problem to the lattice problem in reciprocal space. Here it is important to distinguish between cluster and lattice quantities. The exact lattice self-energy $\Sigma(\mathbf{k})$ given in (4) is the unknown quantity which we wish to approximate. However, let us assume at this stage that we do know a cluster self-energy $\Sigma_{cl}(\mathbf{K}_n)$ (this will in fact be determined later when solving the impurity problem).

The first step in the mapping is to average $\Sigma(\mathbf{k})$ over the momenta $\mathbf{q}$ within each of the $N_c$ tiles, such as those shown in Fig. 1. This results in a *coarse-grained* lattice self-energy $\Sigma(\mathbf{K}_n)$ which has a constant but different value within each tile. On the other hand, the cluster self-energy $\Sigma_{cl}(\mathbf{K}_n)$ is defined only at the cluster momenta $\{\mathbf{K}_n\}$. The main approximation made by the NLCPA [15] is to set $\Sigma(\mathbf{K}_n)$ to be equal to the value $\Sigma_{cl}(\mathbf{K}_n)$ within each tile $n$ i.e.

$$\frac{1}{\Omega_{\mathbf{K}_n}} \int_{\Omega_{\mathbf{K}_n}} d\mathbf{q}\, \Sigma(\mathbf{K}_n + \mathbf{q}) = \Sigma(\mathbf{K}_n) \simeq \Sigma_{cl}(\mathbf{K}_n) \tag{13}$$

In other words, the lattice self-energy is approximated by that obtained from the cluster. Physically, this means that the exact medium described by (4) has been replaced by an effective medium which is still translationally-invariant but the range of nonlocal correlations retained are restricted by the size of the cluster. Note that a precise correlation length can be defined using Nyquist's sampling theorem [15, 29].

The lattice Green's function in reciprocal space may be represented by summing over the dispersion within each tile, yielding the set of coarse-grained values

$$\overline{G}(\mathbf{K}_n) = \frac{N_c}{\Omega_{BZ}} \int_{\Omega_{\mathbf{K}_n}} d\mathbf{k}\, (E - W(\mathbf{k}) - \Sigma(\mathbf{K}_n))^{-1} \tag{14}$$

which are straightforward to calculate since $\Sigma(\mathbf{K}_n)$ is constant within each tile $\Omega_{\mathbf{K}_n}$. This step is consistent with the approximation made above and is carried out to remove phase factors involving lattice momenta. The real space Green's function at the cluster sites can now be obtained using (11) i.e.

$$\overline{G}^{IJ} = \frac{1}{\Omega_{BZ}} \sum_{\mathbf{K}_n} \int_{\Omega_{\mathbf{K}_n}} d\mathbf{k}\, (E - W(\mathbf{k}) - \Sigma(\mathbf{K}_n))^{-1}\, e^{i\mathbf{K}_n(\mathbf{R}_I - \mathbf{R}_J)} \tag{15}$$

**Impurity problem**

At this stage, we have assumed that the cluster self-energy is known. However, in order to determine a cluster self-energy, the impurity problem must be solved. The first step is to define the reciprocal space cavity Green's function $\mathcal{G}(\mathbf{K}_n)$ via the Dyson equation

$$\overline{G}(\mathbf{K}_n) = \mathcal{G}(\mathbf{K}_n) + \mathcal{G}(\mathbf{K}_n)\Sigma(\mathbf{K}_n)\overline{G}(\mathbf{K}_n) \tag{16}$$

In diagrammatic terms $\mathcal{G}(\mathbf{K}_n)$ is introduced to avoid over-counting self-energy diagrams on the cluster [16]. Equation (16) can also be expressed in real space by applying the Fourier transform (11) to yield

$$\overline{G}^{IJ} = \mathcal{G}^{IJ} + \sum_{K,L} \mathcal{G}^{IK}\Sigma^{KL}\overline{G}^{LJ} \tag{17}$$

where $\mathcal{G}^{IJ}$ is the real space cavity Green's function. Significantly, $\mathcal{G}^{IJ}$ is independent of the chemical occupation of the cluster itself. This means the NLCPA impurity cluster Green's function may be defined simply by replacing the cluster self-energy in (17) with a particular configuration of site energies $\{\epsilon_\alpha^I\}$ i.e.

$$G_\gamma^{IJ} = \mathcal{G}^{IJ} + \sum_{K} \mathcal{G}^{IK}\epsilon_\alpha^K G_\gamma^{KJ} \tag{18}$$

The NLCPA self-consistency condition is

$$\sum_\gamma P_\gamma G_\gamma^{IJ} = \overline{G}^{IJ} \tag{19}$$

where $P_\gamma$ is the probability of configuration $\gamma$ occuring (weighted to include SRO if desired). It is important to realise that (19) is the step which implicitly generates the cluster self-energy. The effective medium is therefore determined from a self-consistent solution of (15) and (19). Finally note that the NLCPA formalism reduces to the CPA for $N_c = 1$ and becomes exact as $N_c \to \infty$ since this would amount to solving the exact problem described by (3) and (4).

**Algorithm**

In the following, an underscore denotes a matrix in the cluster-site index. For each energy $E$,

1. For the first iteration, make a guess for the cluster self-energy $\underline{\Sigma}$ e.g. zero.
2. Convert the matrix elements $\Sigma^{IJ}$ to reciprocal space using (11).
3. Calculate the matrix elements $\overline{G}(\mathbf{K}_n)$ using (14) and convert to real space using (11).
4. Calculate the cavity Green's function by solving (17) i.e. $\underline{\mathcal{G}} = \left(\underline{\overline{G}}^{-1} + \underline{\Sigma}\right)^{-1}$.
5. Calculate the impurity Green's function for each of the $2^{N_c}$ impurity cluster configurations via (18).
6. Calculate a new $\underline{\overline{G}}$ by averaging $\underline{G}_\gamma$ over all configurations (with an appropriate weighting to include SRO if required).

7. Using $\underline{\mathcal{G}}$ from step 4 and the new $\underline{\overline{G}}$ from step 6, calculate a new guess at the self-energy via $\underline{\Sigma} = \underline{\mathcal{G}}^{-1} - \underline{\overline{G}}^{-1}$.

8. Compare the new matrix elements $\Sigma^{IJ}$ with those in step 1. If they are not equal to within the desired accuracy, repeat as necessary steps $2 \rightarrow 8$ using the new $\underline{\Sigma}$ until convergence within the desired accuracy is achieved.

**Calculating observables**

Once the medium has been determined through (15) and (19), there is no longer any need to coarse-grain the Green's function via (14). Now, the Green's function may be calculated at any point in the BZ through

$$\overline{G}(\mathbf{k}) = (E - W(\mathbf{k}) - \Sigma(\mathbf{K}_n))^{-1} \tag{20}$$

and correspondingly at any sites $i, j$ in the lattice by

$$\overline{G}^{ij} = \frac{1}{\Omega_{BZ}} \int_{\Omega_{BZ}} d\mathbf{k}\, (E - W(\mathbf{k}) - \Sigma(\mathbf{K}_n))^{-1}\, e^{i\mathbf{k}(\mathbf{R}_i - \mathbf{R}_j)} \tag{21}$$

In (20) and (21) above, $\Sigma(\mathbf{K}_n)$ takes the appropriate value within each tile $n$. The configurationally-averaged DOS per site is given by the usual expression

$$\overline{n}(E) = -\frac{1}{\pi}\, Im\, \overline{G}^{II} \tag{22}$$

where $\overline{G}^{II}$ is independent of the choice of site $I$. However, when calculating site-off diagonal observables such as the spectral function, notice that $\Sigma(\mathbf{K}_n)$ taking the appropriate constant value within each tile in (20) leads to unphysical discontinuities in $\overline{G}(\mathbf{k})$ at the tile boundaries. This point will be addressed and resolved in the following numerical investigation.

**Numerical Investigation**

Due to the numerous possible applications and further conceptual development of the NLCPA method, it is important to carry out a numerical investigation in order to establish that the theory produces physically meaningful results. For example, imposing Born-von Karman boundary conditions on the cluster could introduce fluctuations that have no physical relation to the real system. If it is found that the fluctuations are real, it should then be checked that bulk quantities converge towards the exact result as the cluster sizes increases, and whether this convergence is systematic. In order to answer such questions, a numerical investigation of the NLCPA was recently carried out in [30] for a simple 1D model Hamiltonian with random diagonal disorder and nearest neighbour hopping. This is because in 1D the exact result can be obtained numerically, for example using the negative eigenvalue theorem [31]. Also, fluctuations are much more significant in 1D and so detailed structure is expected in the density of states (DOS) which can be accurately compared with both the exact result and other cluster theories such as the embedded cluster method (ECM) [14] and molecular coherent-potential approximation (MCPA) [32,33]. The MCPA is essentially a self-consistent averaged-supercell calculation and is not computationally feasible for realistic systems, however it should yield meaningful results here for the DOS. The ECM is a non-self-consistent cluster theory, however we would also expect the ECM results to be very similar to

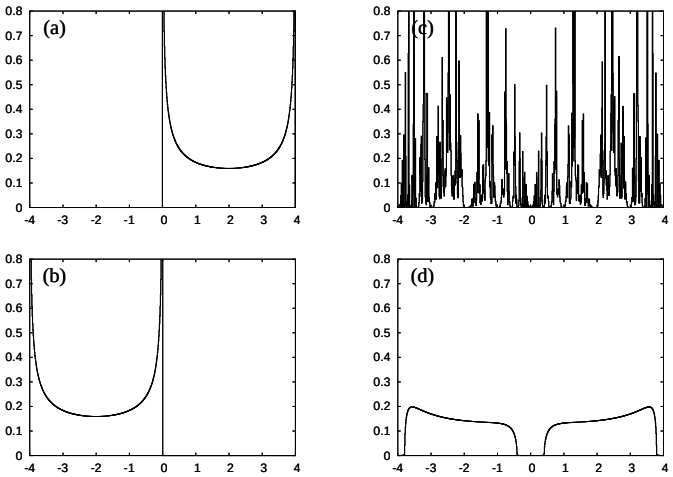


Figure 2: (a) DOS (as a function of energy) for a pure material comprising of $A$ sites, with $\epsilon_A = +2.0$. (b) DOS for a pure material comprising of $B$ sites, with $\epsilon_B = -2.0$. (c) Exact DOS results for a random $A_{50}B_{50}$ alloy of the pure materials above. (d) DOS for the same $A_{50}B_{50}$ alloy obtained using the CPA.

the NLCPA in the absence of chemical short-range order (SRO) since the effects of self-consistency are less signifi cant in the random case.

In summary, it was found in [30] that the NLCPA does produce physically meaningful results, but only above some critical cluster size. To illustrate this, Fig. 2 shows the exact DOS plot for a random (i.e. no SRO) $A_{50}B_{50}$ alloy of constituent site energies $\epsilon_A = +2.0$ and $\epsilon_B = -2.0$ with hopping parameter $W = 1.0$, together with the conventional CPA result. Fig. 3 and Fig. 4 show results for the same model obtained using the ECM (fi rst row), MCPA measured on central site (second row), MCPA averaged over all cluster sites (third row), and the NLCPA with periodic Born-von Karman boundary conditions (fourth row), all as a function of cluster size. It is clear that in the NLCPA calculations for small clusters, there are features present that are not seen elsewhere and appear to be unphysical (for example the troughs present at $E = -3$ and $E = -1.5$ in the $N_c = 2$ calculation). However, such unphysical features are not present for larger cluster sizes and it can be seen that the NLCPA does indeed then converge systematically towards the exact result (note that the ECM converges more quickly here only due to the absence of SRO). However, the apparent unphysical nature of the results for small clusters is an unsatisfactory situation and some solution to the problem is needed.

In order to investigate this problem, calculations were performed in [30] using *anti-periodic* [17] Born-von Karman boundary conditions applied to the cluster instead of the conventional periodic conditions (i.e. quantities at the edges of the cluster map round to minus the value at the opposite edges along each axis). For an infi nite cluster, the periodic and anti-periodic sets of cluster momenta ($\{\mathbf{K}_P\}$ and $\{\mathbf{K}_{AP}\}$ respectively) are equivalent, however as the cluster size decreases, the $\{\mathbf{K}_{AP}\}$ are shifted compared to $\{\mathbf{K}_P\}$ and lie symmetric about the origin (see Fig. 5) for a 1D example with $N_c = 4$). Results obtained using $\{\mathbf{K}_{AP}\}$ are shown in the fi fth row of Fig. 3 and Fig. 4. It can be seen that below a critical cluster size (here $N_c = 12$) the periodic and anti-periodic results diverge and gain unphysical features, although both become equivalent and equal the CPA result at $N_c = 1$. This suggests that when using the NLCPA for cluster sizes $1 < N_c < N_{critical}$, a way forward is to appropriately mix the periodic and anti-periodic results to produce a new unique solution.

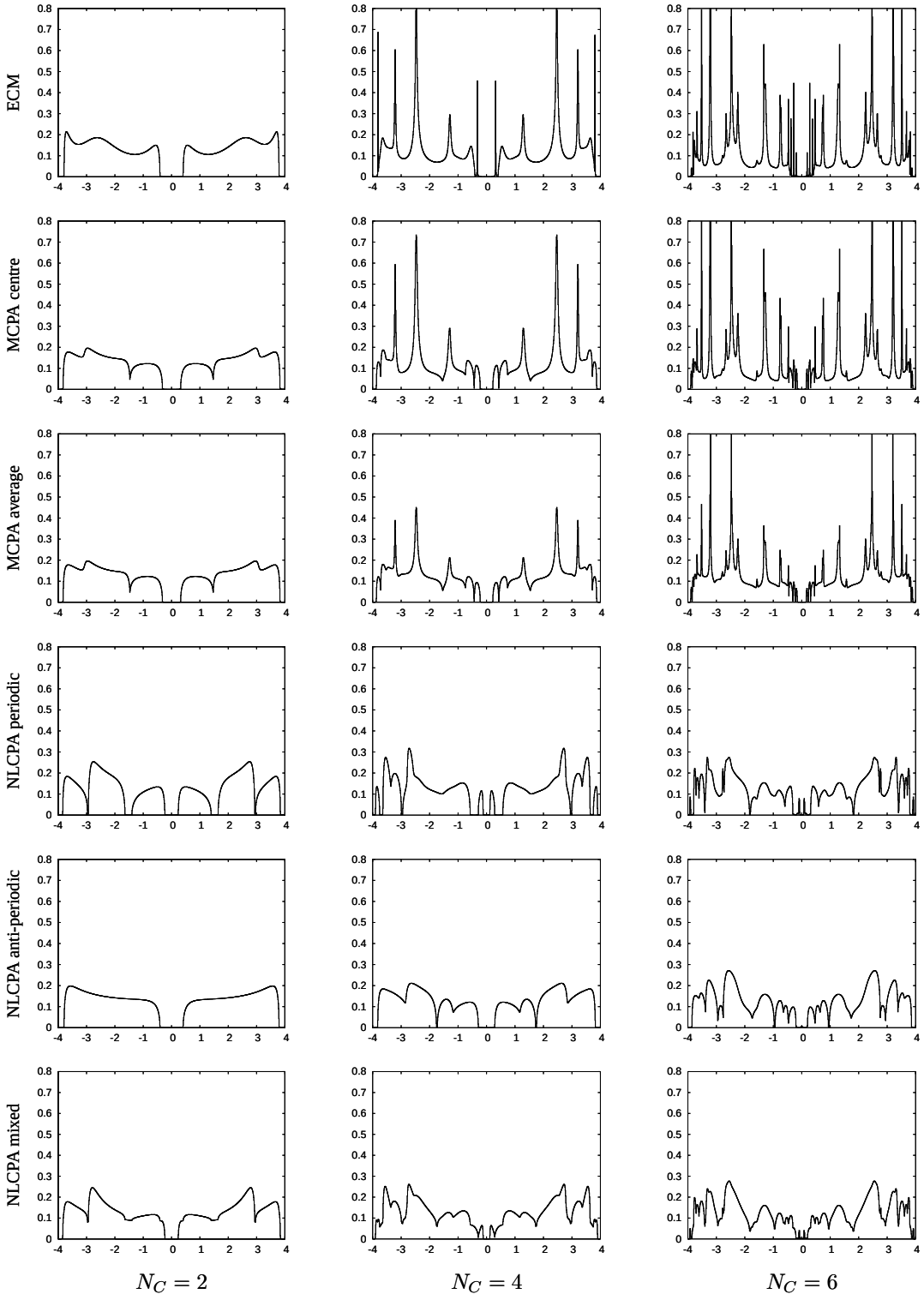


Figure 3: Confi gurationally-averaged DOS per site as a function of energy (in units of the bandwidth) for the various cluster theories (top to bottom) with cluster sizes $N_c = 2, 4, 6$ (left to right).

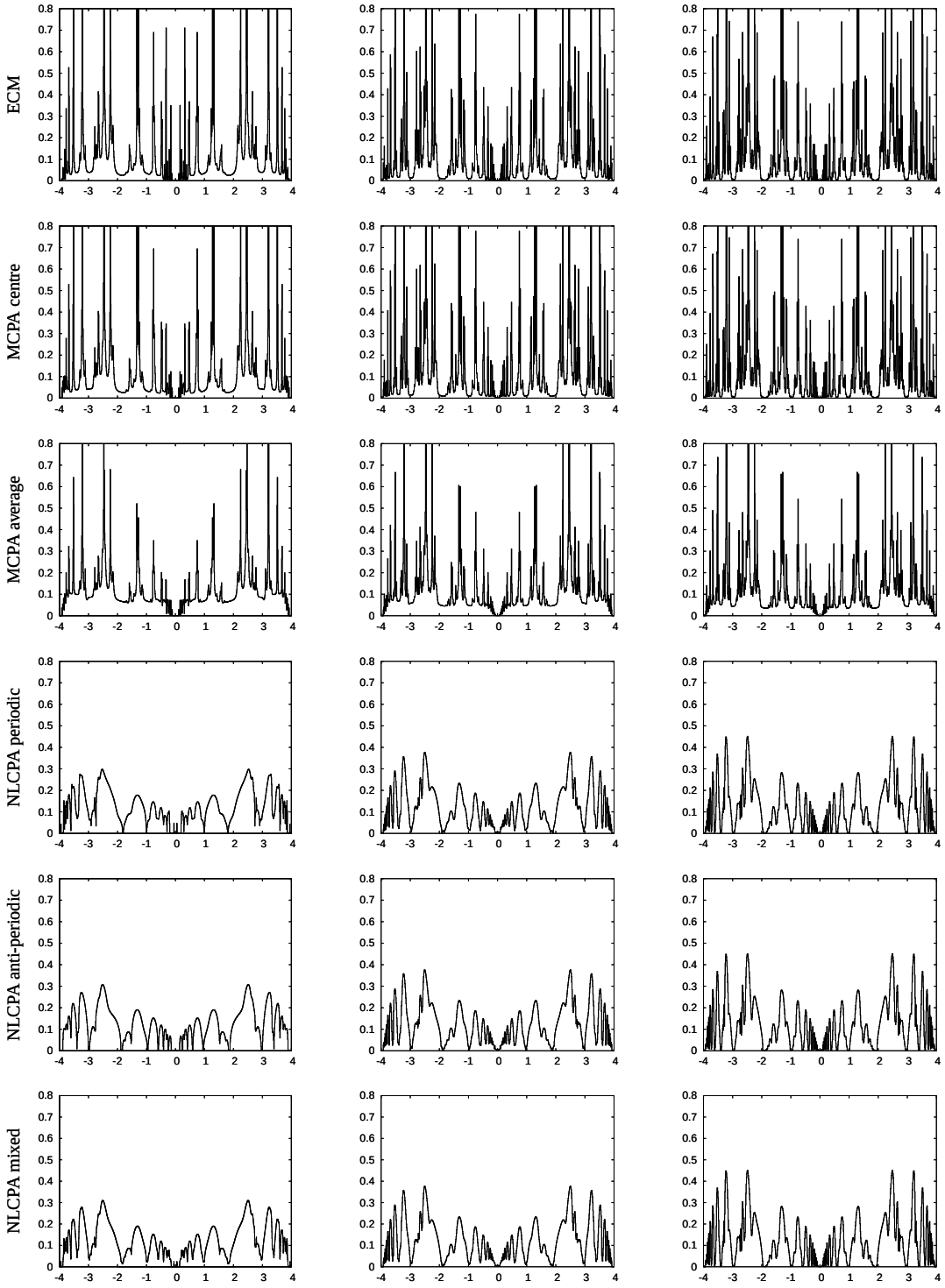


Figure 4: Configurationally-averaged DOS per site as a function of energy (in units of the bandwidth) for the various cluster theories (top to bottom) with cluster sizes $N_c = 8, 12, 16$ (left to right).

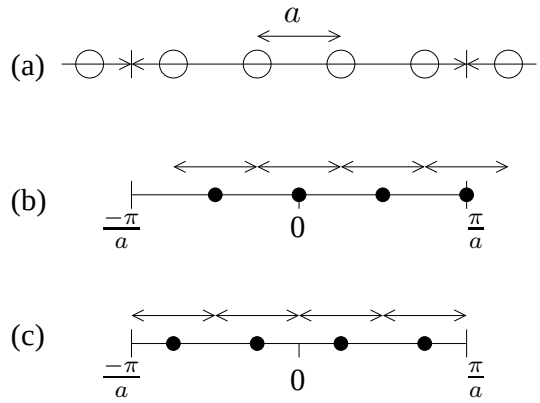


Figure 5: (a) Real space tile (denoted by double-headed arrow of length $4a$) for a $N_c = 4$ cluster in 1D. Sites are denoted by open circles, and $a$ is the lattice constant. (b) Set of cluster momenta (periodic) denoted by closed circles for the $N_c = 4$ cluster. The tiles centred at the cluster momenta are denoted by arrows and the solid line is the first BZ. The part of the tile centred at $\pi/a$ that lies outside the first BZ can be translated by reciprocal lattice vectors into the first BZ to lie between $-\pi/a$ and $-\pi/4a$. (c) Set of cluster momenta (anti-periodic) denoted by closed circles for the $N_c = 4$ cluster. Again the tiles centred at the cluster momenta are denoted by arrows and the solid line is the first BZ.

Let us begin by labelling the Green's function (given by (20)) for the periodic and anti-periodic solutions by $\overline{G}_P(\mathbf{k})$ and $\overline{G}_{AP}(\mathbf{k})$ respectively. Next, observe that on account of the coarse-graining procedure outlined earlier, by construction $\overline{G}_P(\mathbf{k})$ is a better approximation to the exact result in the region of reciprocal space close to each of the points $\{\mathbf{K}_n^P\}$ (in fact $\overline{G}_{AP}(\mathbf{k})$ has discontinuities at $\{\mathbf{K}_n^P\}$). Similarly $\overline{G}_{AP}(\mathbf{k})$ is a better approximation to the exact result close to each of the points $\{\mathbf{K}_n^{AP}\}$. This suggests that one should construct a new mixed Green's function $\overline{G}_M(\mathbf{k})$ which follows $\overline{G}_P(\mathbf{k})$ close to each of the points $\{\mathbf{K}_n^P\}$, and follows $\overline{G}_{AP}(\mathbf{k})$ close to each of the points $\{\mathbf{K}_n^{AP}\}$. A method for carrying out this has been proposed in [34]. By defining a mixing parameter which is subject to conditions at the tile boundaries, such a problem can be directly mapped to that of the potential of a static membrane, the minimization of which gives the well known Laplace equation describing wave motion. For example, in 1D this yields the simple expression

$$\overline{G}_M(\mathbf{k}) = \overline{G}_P(\mathbf{k}) \cos^2\left((N_c a/2)\mathbf{k}\right) + \overline{G}_{AP}(\mathbf{k}) \sin^2\left((N_c a/2)\mathbf{k}\right) \tag{23}$$

for the new mixed Green's function. The final row in Fig. 3 and Fig. 4 show DOS results using (23). Reassuringly, the new mixed NLCPA result looks remarkably similar to both the ECM and MCPA results for all cluster sizes, with unphysical features removed and troughs and peaks in the DOS which can be associated with specific cluster disorder configurations.

In conclusion, when using the NLCPA one should first establish the critical cluster size $N_{critical}$ for the model in question i.e. the smallest cluster for which the periodic and anti-periodic results are equivalent. For $N_c \geq N_{critical}$ the result is independent of the boundary condition and thus the conventional periodic results may be used. For calculations with $1 < N_c < N_{critical}$, the method proposed in [34] should be used to mix the periodic and anti-periodic results. Note that the method is perfectly general and can be applied to any (allowed) cluster in any dimension.

**Spectral function in the NLCPA**

The success of the method of [34] mentioned above for mixing the periodic and anti-periodic solutions is due to the fact that in addition to effectively increasing the number of cluster momenta in the BZ (see Fig. 5), it removes the problem of discontinuities in the self-energy and Green's function since no individual solution is followed where it has a discontinuity. Therefore the mixed Green's function $\overline{G}_M(\mathbf{k})$ has its own associated self-energy which is fully $\mathbf{k}$-dependent and continuous. In addition to yielding unique, meaningful, and systematic results, the method therefore also yields a well-defined spectral function

$$A_B^M(\mathbf{k},\epsilon) = -\frac{1}{\pi} Im\, \overline{G}_M(\mathbf{k},\epsilon) \tag{24}$$

which can be used to calculate Fermi surfaces. Some spectacular new Fermi surface features obtained using the method (such as new nesting features and an electronic topological transition not predicted by the conventional CPA) are illustrated in [34] for a 2D tight-binding model. Clearly, it would be beneficial to apply the method within first-principles KKR calculations. A derivation and implementation of the spectral function has recently been given within the first-principles KKR-NLCPA multiple-scattering theory in [35], although only the periodic set of cluster momenta are used and no attempt is made to remove the discontinuities. The formalism of [35] combined with that of [34] would enable the effects of SRO to be studied on interesting Fermi surface features of systems such as $CuPd$ [27].

# 3 KKR-NLCPA

**Brief introduction to KKR theory**

The aim of a first-principles electronic structure method is to solve the Kohn-Sham equation. Instead of calculating the charge density from the single-electron Kohn-Sham states, the KKR method uses the corresponding single-electron multiple-scattering Green's function. To do this, the usual Dyson equation in operator form $(G = G_0 + G_0 V G)$ is rewritten as

$$G = G_0 + G_0 T G_0 \tag{25}$$

where the multiple scattering $T$ operator has been defined by $VG = TG_0$ and describes all possible scattering in the system as it relates the free-particle Green's operator to the full scattering Green's operator. The basic idea is to represent the multiple-scattering problem in terms of the scattering properties of the individual sites. By decomposing the effective Kohn-Sham potential into contributions from individual sites, it can be shown that the transition operator $T$ can be written in terms of the multiple scattering operator $\tau^{ij}$ by $T = \sum_{ij} \tau^{ij}$ where

$$\tau^{ij} = t^i \delta_{ij} + \sum_{k \neq i} t^i G_0^{ik} t^k \delta_{kj} + \sum_{k \neq i} \sum_{l \neq k} t^i G_0^{ik} t^k G_0^{kl} t^l \delta_{lj} + \cdots = t^i \delta_{ij} + \sum_{k \neq i} t^i G_0^{ik} \tau^{kj} \tag{26}$$

Here the single-site $t$-operators describe the scattering at each individual site and $G_0$ the free-space propagation of an electron in between scattering events. So $\tau^{ij}$ gives the scattered wave from site $i$ due to a wave incident upon site $j$, taking into account all possible scatterings in between.

For computational purposes, we need to go into a coordinate and angular momentum representation. In a coordinate representation, the effective potential $V(\mathbf{r})$ is taken as a sum of non-overlapping spherical

contributions $V_i(\mathbf{r}-\mathbf{R}_i)$ centred at each site $\mathbf{R}_i$, and is set equal to zero or a constant in the interstitial region outside these 'muffi n-tin' spheres. Then by performing a partial wave decomposition, (25) and (26) eventually become

$$G(\mathbf{r},\mathbf{r}',E)=\sum_L Z_L(\mathbf{r}_i,E)\tau^{ij}_{LL'}(E)Z_{L'}(\mathbf{r'}_j,E)-\delta_{ij}\sum_L Z_L(\mathbf{r}_i^<,E)\tilde{J}_L(\mathbf{r}_i^>,E) \tag{27}$$

$$\tau^{ij}_{LL'}(E)=t^i_L(E)\delta_{ij}\delta_{LL'}+\sum_{k\neq i}\sum_{L''}t^i_L(E)G_{0,LL''}(\mathbf{R}_i-\mathbf{R}_k,E)\tau^{kj}_{L''L'}(E) \tag{28}$$

respectively, where $\mathbf{r}=\mathbf{r}_i+\mathbf{R}_i$ is restricted to lie in the $i^{th}$ bounding sphere and $\mathbf{r}'=\mathbf{r'}_j+\mathbf{R}_j$ in the $j^{th}$ sphere, and $L=\{l,m\}$ is the angular momentum index. The free-space structure constants $G_{0,LL''}(\mathbf{R}_i-\mathbf{R}_k,E)$ describing the free-particle propagation in between scattering events depend on the structure of the lattice only. $Z_L(\mathbf{r}_i,E)$ is the solution of the single-site Schrödinger equation at site $i$ that is regular at the origin and must join smoothly to a linear combination of free-particle solutions at the muffi n-tin boundary. Using the normalisation of Ref. [36], this combination is taken to be

$$Z_L(\mathbf{r},E)=J_L(\mathbf{r},E)t_L^{-1}(E)-ikH_L(\mathbf{r},E) \tag{29}$$

where $k=\sqrt{2mE/\hbar^2}$, $J_L(\mathbf{r},E)=j_l(r,E)Y_l^m(\widehat{r})$, and $H_L(\mathbf{r},E)=h_l(r,E)Y_l^m(\widehat{r})$. In (27), $\tilde{J}_L(\mathbf{r},E)$ is the solution of the single-site Schrödinger equation at site $i$ that is irregular at the origin and must join must join smoothly to the free particle solution $J_L(\mathbf{r},E)$ at the muffi n-tin boundary. Equation (29) also defi nes the single-site t-matrix, which is related to the phase shift by

$$t_L(E)=-\frac{1}{\sqrt{E}}\sin\delta_L(E)e^{i\delta_L} \tag{30}$$

For clarity, (28) may be written in the form

$$\underline{\tau}^{ij}=\underline{t}^i\delta_{ij}+\sum_{k\neq i}\underline{t}^i\underline{G}(\mathbf{R}_{ik})\underline{\tau}^{kj} \tag{31}$$

where the underscore denotes a matrix in the angular momentum index (usually cut off at $L=2$ or 3). For translationally-invariant systems (31) may be expressed in reciprocal space as

$$\underline{\tau}(\mathbf{k})=\underline{t}+\underline{t}\,\underline{G}(\mathbf{k})\,\underline{\tau}(\mathbf{k})=\left(\underline{t}^{-1}-\underline{G}(\mathbf{k})\right)^{-1} \tag{32}$$

Therefore once the t-matrix and structure constants are known, the matrix elements $\underline{\tau}^{ij}$ may be calculated via the BZ integral

$$\underline{\tau}^{ij}=\frac{1}{\Omega_{BZ}}\int d\mathbf{k}\left(\underline{t}^{-1}-\underline{G}(\mathbf{k})\right)^{-1}e^{i\mathbf{k}(\mathbf{R}_i-\mathbf{R}_j)} \tag{33}$$

The Green's function may then be calculated via (27) from which observables can be found. For example, the charge density is given by

$$\rho(\mathbf{r})=-\frac{1}{\pi}Im\int_{-\infty}^{E_F}G(\mathbf{r},\mathbf{r},E)dE \tag{34}$$

for reconstructing the effective potential $V(\mathbf{r})$ in the DFT self-consistency loop.

**Self-Consistent-Field (SCF)-KKR-CPA**

In principle, a DFT calculation for a disordered system means that self-consistency with respect to the electronic charge distribution should be achieved for each disorder configuration individually and then an average taken over all disorder configurations. This is clearly intractable, and so the strategy behind the SCF-KKR-CPA [8, 9] is to enforce charge self-consistency only with respect to single-site *partially-averaged* charge densities $\rho_\alpha$, such single-site partial averages being the constrained average over all configurations which leave the occupancy of a single site of chemical type $\alpha$ fixed [8, 9]. The Kohn-Sham effective potential $V_\alpha$ is taken to depend only on $\rho_\alpha$ on the fixed site and the average charge density $\sum_\alpha \rho_\alpha$ on all other sites. So for a binary alloy, self-consistency is achieved when the partially-averaged charge densities $\rho_A$ and $\rho_B$ are consistent with the effective potentials $V_A$ and $V_B$. Note that the total energy is expressed as a functional of the $\{\rho_\alpha\}$ and is stationary with respect to them [11], which is one of the main reasons behind the success of the method.

Let us assume that we are given two output effective potentials $V_A$ and $V_B$. From these, we can calculate the single-site $t$-matrices $\underline{t}_A$ and $\underline{t}_B$. The KKR-CPA must now be used to perform the configurational averaging. To do this, we proceed in analogy to the derivation of the CPA within the tight-binding framework in Section 2. The KKR-CPA assumes a translationally-invariant effective medium comprising of identical effective scatterers $\underline{\bar{t}}$ placed on every site. The effective scattering path matrix $\underline{\overline{\tau}}^{ij}$ describing such a medium is given by

$$\underline{\overline{\tau}}^{ij} = \underline{\bar{t}}^{\,i}\,\delta_{ij} + \sum_{k\neq i} \underline{\bar{t}}^{\,i}\,\underline{G}(\mathbf{R}_{ik})\underline{\overline{\tau}}^{kj} \tag{35}$$

In order to determine the medium, consider a site $i$. By removing the sum over all sites $k$ and making up for the neglected terms by introducing the renormalised interactor $\underline{\overline{\Delta}}^{ii}$, the site-diagonal part of (35) at site $i$ can be formally rewritten in the form

$$\underline{\overline{\tau}}^{ii} = \underline{\bar{t}}^{\,i}\,\delta_{ij} + \underline{\bar{t}}^{\,i}\,\underline{\overline{\Delta}}^{ii}\underline{\overline{\tau}}^{ii} \;=\; \left(\underline{\bar{t}}^{\,i\,-1} - \underline{\overline{\Delta}}^{ii}\right)^{-1} \tag{36}$$

where the renormalised interactor $\underline{\overline{\Delta}}^{ii}$ can be written in terms of an expansion over the remaining lattice sites [14]. Since $\underline{\overline{\Delta}}^{ii}$ describes the interaction of site $i$ with the rest of the medium i.e. describes all paths starting and ending on site $i$ which avoid site $i$ at all intermediate steps, it is independent of the nature of the potential at site $i$. It is therefore straightforward to define the path matrix for paths starting and ending on a real *impurity* embedded in the medium simply by replacing the effective scatterer $\underline{\bar{t}}$ with a real $t$-matrix $\underline{t}^i_\alpha$ at site $i$, where $\alpha = A$ or $B$. From (36) this is given by

$$\underline{\tau}^{ii}_\alpha = \left(\underline{t}^{\,i\;-1}_\alpha - \underline{\overline{\Delta}}^{ii}\right)^{-1} = \left[\underline{\overline{\tau}}^{ii\,-1} + \underline{t}^{\,i\;-1}_\alpha - \underline{\bar{t}}^{\,i\,-1}\right]^{-1} \tag{37}$$

The KKR-CPA requires that

$$\sum_\alpha P_\alpha \underline{\tau}^{ii}_\alpha = \underline{\overline{\tau}}^{ii} \tag{38}$$

where $P_\alpha$ is the probability that site $i$ is of chemical type $\alpha$. In other words, there should be no excess scattering from the impurity site on the average. Since we require the KKR-CPA effective medium to be translationally-invariant, $\underline{\overline{\tau}}^{ii}$ must also satisfy the BZ integral

$$\underline{\overline{\tau}}^{ii} = \frac{1}{\Omega_{BZ}} \int_{\Omega_{BZ}} d\mathbf{k} \left(\underline{\bar{t}}^{-1} - G(\mathbf{k})\right)^{-1} \tag{39}$$

The KKR-CPA medium is therefore determined from a self-consistent solution of (38) and (39). After the medium has been determined, the site-diagonal part of the Green's function (27) for an impurity site embedded in the medium is given by

$$G_\alpha(E,\mathbf{r}_i,\mathbf{r}'_i) = \sum_{LL'} P_\alpha Z^\alpha_L(E,\mathbf{r}_i)\tau^{ii}_{\alpha,LL'} Z^i_{L'}(E,\mathbf{r}'_i) - \sum_L P_\alpha Z^\alpha_L(E,\mathbf{r}_i)\tilde{J}^\alpha_L(E,\mathbf{r}'_i) \tag{40}$$

where $\alpha$ denotes a site of type $A$ or $B$, and $\tau^{ii}_{\alpha,LL'}$ is given by (37). The total average Green's function is then given by summing over $\alpha$. However, from (40) we can calculate the charge density at the impurity site via

$$\rho_\alpha(\mathbf{r}_i) = -\frac{1}{\pi} Im \int_{-\infty}^{E_F} G_\alpha(E,\mathbf{r}_i,\mathbf{r}_i) dE \tag{41}$$

This is the CPA approximation to the single-site partially-averaged charge density since it is the charge density for a fixed site embedded in a (mean-field) averaged environment. Using $\rho_\alpha$ on the fixed site and the average charge density $\sum_\alpha \rho_\alpha$ on all other sites, new effective potentials $\{V_\alpha\}$ can be contructed for feeding back to the DFT self-consistency loop [8, 9].

**'First-Pass' KKR-NLCPA**

The key step in deriving the NLCPA within the KKR multiple scattering framework is to identify the quantities which played the role of the self-energy $\Sigma^{ij}$ in the derivation within the tight-binding framework in Section 2. It is clear that there is a direct analogy between the single-site t-matrices $\underline{t}^i$ and the site energies $\epsilon^i$, and similarly between the free-space structure constants $\underline{G}(\mathbf{R}_{ij})$ and the hopping terms $W^{ij}$. This implies that for the site-diagonal part of $\Sigma^{ij}$, which describes an effective on-site energy, there is a clear analogy to an effective single-site t-matrix $\underline{\widehat{t}}^i$. For the site off-diagonal part of $\Sigma^{ij}$, which from (4) describes an effective correction to the hopping, it follows that we need to introduce a new effective correction $\underline{\widehat{\delta G}}(\mathbf{R}_{ij})$ to the free-space structure constants $\underline{G}(\mathbf{R}_{ij})$. Of course, in the conventional KKR-CPA theory such corrections are never present since the 'coherent-potential' is a single-site quantity, analogous to a single-site self-energy $\Sigma^{ii}$ only within the tight-binding framework.

However, there are important differences in the physical interpretation of the above quantities. Recall that one of the main advantages of the multiple scattering formalism (which for disordered systems facilitates its combination with DFT) is that there is a complete separation between the potential and structural information. The free-space structure constants contain information about the structure of the lattice only; all potential information is contained within the single-site t-matrices. This means that the new effective structure constant corrections $\underline{\widehat{\delta G}}(\mathbf{R}_{ij})$ are limited to describing nonlocal *scattering correlations* only. In other words, in between scattering events, an electron now propagates though a reference medium which is no longer free space. This medium takes into account, on average, the effect on the propagation of the electron due to multiple scatterings from specific disorder configurations. Note that such scattering correlations are present even in the absence of chemical SRO.

Nonlocal *charge correlations* which arise due to the transfer of charge between sites of differing atomic species can be taken into account by combination with DFT i.e. when the potentials are self-consistently determined. Possible charge transfer will then manifest itself by changes to the t-matrices which are fed to the KKR-NLCPA. However, the treatment of charge correlations will not be considered in this section. Here we will simply assume that we have two t-matrices $\underline{t}_A$ and $\underline{t}_B$, for example corresponding to potentials that have been determined self-consistently by the SCF-KKR-CPA described above. The

aim is therefore only to do a 'first-pass' KKR-NLCPA calculation to demonstrate the differences in the resulting effective medium when using the KKR-NLCPA compared to the conventional KKR-CPA.

Given the comments above, the scattering path matrix $\underline{\widehat{\tau}}^{ij}$ for a medium describing the average motion of an electron from site $i$ to site $j$ exactly is defined by

$$\underline{\widehat{\tau}}^{ij} = \underline{\widehat{t}}\,\delta_{ij} + \sum_{k\neq i} \underline{\widehat{t}}\,\left(\underline{G}(\mathbf{R}_{ik}) + \underline{\widehat{\delta G}}(\mathbf{R}_{ik})\right)\underline{\widehat{\tau}}^{kj} \tag{42}$$

Here a circumflex symbol denotes an effective medium quantity, an underscore denotes a matrix in angular momentum space, and the indices $i, j$ run over all sites in the lattice. This equation can be seen as analagous to (3). Since (42) is translationally-invariant, the matrix elements $\underline{\widehat{\tau}}^{ij}$ are also given by the BZ integral

$$\underline{\widehat{\tau}}^{ij} = \frac{1}{\Omega_{BZ}}\int_{\Omega_{BZ}} d\mathbf{k}\left(\underline{\widehat{m}} - \underline{\widehat{\delta G}}(\mathbf{k}) - \underline{G}(\mathbf{k})\right)^{-1} e^{i\mathbf{k}(\mathbf{R}_i-\mathbf{R}_j)} \tag{43}$$

where $\underline{\widehat{m}} = \underline{\widehat{t}}^{-1}$. By comparing (5) and (43), it is clear that the role of $\Sigma(\mathbf{k})$ is played by $-(\underline{\widehat{m}} - \underline{\delta G}(\mathbf{k}))$. Following the derivation given in Section 2, the next step is to select an appropriate cluster and tile (see later in this section for more details), apply Born-von Karman boundary conditions to the cluster, and find the corresponding set of cluster sites $\{I\}$ and cluster momenta $\{\mathbf{K}_n\}$ satisfying (11). Then let us assume that we know the cluster quantities

$$\begin{aligned}\left(\underline{\widehat{m}}^I\delta_{IJ} - \underline{\widehat{\delta G}}(\mathbf{R}_{IJ})\right) &= \frac{1}{N_c}\sum_{\mathbf{K}_n}\left(\underline{\widehat{m}} - \underline{\widehat{\delta G}}(\mathbf{K}_n)\right)e^{i\mathbf{K}_n(\mathbf{R}_I-\mathbf{R}_J)} \\ \left(\underline{\widehat{m}} - \underline{\widehat{\delta G}}(\mathbf{K}_n)\right) &= \sum_{J}\left(\underline{\widehat{m}}^I\delta_{IJ} - \underline{\widehat{\delta G}}(\mathbf{R}_{IJ})\right)e^{-i\mathbf{K}_n(\mathbf{R}_I-\mathbf{R}_J)}\end{aligned} \tag{44}$$

which are analagous to $\Sigma_{cl}^{IJ}$ and $\Sigma_{cl}(\mathbf{K}_n)$. Now the cluster can be mapped to the lattice in reciprocal space in exactly the same way as Section 2 i.e. the scattering path matrix is represented by the set of coarse-grained values

$$\underline{\widehat{\tau}}(\mathbf{K}_n) = \frac{N_c}{\Omega_{BZ}}\int_{\Omega_{\mathbf{K}_n}} d\mathbf{k}\left(\underline{\widehat{m}} - \underline{\widehat{\delta G}}(\mathbf{K}_n) - \underline{G}(\mathbf{k})\right)^{-1} \tag{45}$$

and by using (11) the scattering path matrix at the cluster sites becomes

$$\underline{\widehat{\tau}}^{IJ} = \frac{1}{\Omega_{BZ}}\sum_{\mathbf{K}_n}\left(\int_{\Omega_{\mathbf{K}_n}} d\mathbf{k}\left(\underline{\widehat{m}} - \underline{\widehat{\delta G}}(\mathbf{K}_n) - \underline{G}(\mathbf{k})\right)^{-1}\right)e^{i\mathbf{K}_n(\mathbf{R}_I-\mathbf{R}_J)} \tag{46}$$

Again, physically this means that the 'exact' medium described by (42) has been replaced by an effective medium which is still translationally-invariant but the range of nonlocal correlations retained (described by $\underline{\widehat{\delta G}}(\mathbf{R}_{IJ})$) are restricted by the size of the cluster used to determine the medium. However, the above mapping was based on the assumption that we know the quantities in (44). To determine them, the impurity problem must be solved by generalising the conventional KKR-CPA argument in real space. This can be straightforwardly done by rearranging (42) for the effective medium in the form

$$\underline{\widehat{\tau}}^{IJ} = \underline{\widehat{t}}_{cl}^{\,IJ} + \sum_{K,L}\underline{\widehat{t}}_{cl}^{\,IK}\,\underline{\widehat{\Delta}}^{KL}\,\underline{\widehat{\tau}}^{LJ} \tag{47}$$

where the effective cluster t-matrix is defined by

$$\underline{\widehat{t}}_{cl}^{\,IJ} = \underline{\widehat{t}}^{\,I}\,\delta_{IJ} + \sum_{K}\underline{\widehat{t}}^{\,I}\left(\underline{G}(\mathbf{R}_{IK}) + \underline{\widehat{\delta G}}(\mathbf{R}_{IK})\right)\underline{\widehat{t}}_{cl}^{\,KJ} \tag{48}$$

and describes all scattering within the cluster, whilst the cavity function $\underline{\widehat{\Delta}}^{IJ}$ describes all scattering outside of the cluster. Since $\underline{\widehat{\Delta}}^{IJ}$ describes the medium outside and is independent of the contents of the cluster, it may be used to define the impurity cluster path matrix

$$\underline{\tau}_{\gamma}^{IJ} = \underline{t}_{cl,\gamma}^{IJ} + \sum_{K,L} \underline{t}_{cl,\gamma}^{IK}\, \underline{\Delta}^{KL}\, \underline{\tau}_{\gamma}^{LJ} \tag{49}$$

where the impurity cluster t-matrix is defined by

$$\underline{t}_{cl,\gamma}^{IJ} = \underline{t}_{\gamma}^{I}\delta_{IJ} + \sum_{K} \underline{t}_{\gamma}^{I}\, \underline{G}(\mathbf{R}_{IK})\, \underline{t}_{cl}^{KJ}. \tag{50}$$

for a fixed impurity cluster configuration $\gamma$. In other words, the effective cluster has simply been replaced by an 'impurity' cluster of real t-matrices with configuration $\gamma$ and free-space structure constants 'embedded' in the (still undetermined) effective medium. The KKR-NLCPA self-consistency condition demands that there be no additional scattering from the cluster on the average i.e.

$$\sum_{\gamma} P_{\gamma}\, \underline{\tau}_{\gamma}^{IJ} = \underline{\widehat{\tau}}^{IJ}, \tag{51}$$

where $P_{\gamma}$ is the probability of configuration $\gamma$ occuring. The effective medium t-matrices and structure constant corrections are thus determined from a self-consistent solution of (46) and (51). After the medium has been determined, the site-diagonal part of the Green's function (27) for any site $I$ belonging to an impurity cluster of configuration $\gamma$ embedded in the medium is given by

$$G_{\gamma}(E, \mathbf{r}_I, \mathbf{r}'_I) = \sum_{LL'} P_{\gamma} Z_L^{\gamma}(E, \mathbf{r}_I) \tau_{\gamma, LL'}^{II} Z_{L'}^{I}(E, \mathbf{r}'_I) - \sum_{L} P_{\gamma} Z_L^{\gamma}(E, \mathbf{r}_I) \tilde{J}_L^{\gamma}(E, \mathbf{r}'_I) \tag{52}$$

Therefore the partially-averaged cluster charge density measured at the site $I$, given that the cluster configuration is $\gamma$, is obtained from

$$\rho_{\gamma}(\mathbf{r}_I) = -\frac{1}{\pi} Im \int_{-\infty}^{E_F} G_{\gamma}(E, \mathbf{r}_I, \mathbf{r}_I) dE \tag{53}$$

The total average Green's function and charge densities are obtained by summing over all $\gamma$, and any site in the cluster can be chosen to be site $I$ since all cluster sites are equivalent after averaging over all $\gamma$.

**KKR-NLCPA algorithm**

For computational purposes it is not necessary to involve $\underline{\widehat{t}}_{cl}^{IJ}$ since this quantity includes the free-space structure constants which are not strictly needed (although they should be included in the formal multiple scattering derivation as above in order to facilitate the scattering within the cluster). Instead, it is easier to leave the free space structure constants inside the cavity i.e. renormalise $\underline{\underline{\widehat{\Delta}}} + \underline{\underline{G}} \rightarrow \underline{\underline{\widehat{\Delta}}}$ and simply work with the quantity $\underline{\underline{\widehat{m}}} - \underline{\underline{\widehat{\delta G}}}$. For clarity, it is convenient to label this quantity as $\underline{\underline{\widehat{X}}}$ so that $\underline{\widehat{X}}^{IJ} = \underline{\widehat{m}}\delta_{IJ} - \underline{\widehat{\delta G}}(\mathbf{R}_{IJ})(1-\delta_{IJ})$. All real-space matrices in the algorithm are matrices in the cluster site and angular momentum index only (denoted by a double underscore) and all reciprocal-space matrices are diagonal i.e.

$$\underline{\underline{\widehat{X}}} = \begin{bmatrix} \underline{\widehat{X}}^{11} & \underline{\widehat{X}}^{12} & \underline{\widehat{X}}^{13} \cdots \\ \underline{\widehat{X}}^{21} & \underline{\widehat{X}}^{22} & \underline{\widehat{X}}^{23} \cdots \\ \underline{\widehat{X}}^{31} & \underline{\widehat{X}}^{32} & \underline{\widehat{X}}^{33} \ddots \end{bmatrix} = \begin{bmatrix} \underline{\widehat{m}} & \underline{\widehat{\delta G}}(\mathbf{R}_{12}) & \underline{\widehat{\delta G}}(\mathbf{R}_{13}) \cdots \\ \underline{\widehat{\delta G}}(\mathbf{R}_{21}) & \underline{\widehat{m}} & \underline{\widehat{\delta G}}(\mathbf{R}_{23}) \cdots \\ \underline{\widehat{\delta G}}(\mathbf{R}_{31}) & \underline{\widehat{\delta G}}(\mathbf{R}_{32}) & \underline{\widehat{m}} \ddots \end{bmatrix}$$

$$\underline{\underline{\widehat{X}}}(\mathbf{K}) = \begin{bmatrix} \underline{\widehat{X}}(\mathbf{K}_1) & 0 & 0\cdots \\ 0 & \underline{\widehat{X}}(\mathbf{K}_2) & 0\cdots \\ 0 & 0 & \underline{\widehat{X}}(\mathbf{K}_3)_{\ddots} \end{bmatrix} = \begin{bmatrix} \underline{\widehat{m}} - \underline{\widehat{\delta G}}(\mathbf{K}_1) & 0 & 0\cdots \\ 0 & \underline{\widehat{m}} - \underline{\widehat{\delta G}}(\mathbf{K}_2) & 0\cdots \\ 0 & 0 & \underline{\widehat{m}} - \underline{\widehat{\delta G}}(\mathbf{K}_3)_{\ddots} \end{bmatrix}$$

An example algorithm proceeds as follows:

1. For the first iteration make a guess for the effective matrix $\underline{\widehat{X}}^{IJ}$. For example place an average t-matrix (ATA) $\underline{\overline{t}} = P(A)\underline{t}^A + P(B)\underline{t}^B$ on each cluster site and set the off-diagonal terms $\underline{\widehat{\delta G}}(\mathbf{R}_{IJ})$ to zero.
2. Convert the matrix elements $\underline{\widehat{X}}^{IJ}$ to reciprocal space using (11).
3. Calculate the matrix elements $\underline{\widehat{\tau}}(\mathbf{K}_n)$ via $\underline{\widehat{\tau}}(\mathbf{K}_n) = \frac{N_c}{\Omega_{BZ}} \int_{\Omega_{\mathbf{K}_n}} d\mathbf{k} \left( \underline{\widehat{X}}(\mathbf{K}_n) - \underline{G}(\mathbf{k}) \right)^{-1}$ and convert to real space using (11).
4. Calculate the matrix elements $\underline{\widehat{\Delta}}^{IJ}$ by solving $\underline{\underline{\widehat{\Delta}}} = \underline{\underline{\widehat{X}}} - \underline{\underline{\widehat{\tau}}}^{-1}$.
5. Calculate $\underline{\tau}_\gamma^{IJ}$ for each impurity cluster configuration using $\underline{\underline{\tau}}_\gamma = \left( \underline{\underline{m}}_\gamma - \underline{\underline{\widehat{\Delta}}} \right)^{-1}$
6. Average $\underline{\tau}_\gamma^{IJ}$ over all $2^{N_c}$ configurations (with an appropriate probability distribution to include SRO if desired) to obtain a new effective path matrix at the cluster sites $\underline{\widehat{\tau}}^{IJ}$.
7. Calculate the new effective matrix elements $\underline{\widehat{X}}^{IJ}$ via $\underline{\underline{\widehat{X}}} = \underline{\underline{\widehat{\tau}}}^{-1} + \underline{\underline{\widehat{\Delta}}}$ using $\underline{\underline{\widehat{\Delta}}}$ from step 4 and $\underline{\underline{\widehat{\tau}}}$ from step 6. Note that the off-diagonal matrix elements of the new effective matrix $\underline{\underline{\widehat{X}}}$ will no longer be zero due to the configurational averaging in step 6.
8. Compare the new matrix elements $\underline{\widehat{X}}^{IJ}$ with those in step 1. If they are not equal to within the desired accuracy, repeat as necessary steps $2 \rightarrow 8$ using the new $\underline{\widehat{X}}^{IJ}$ until convergence within the desired accuracy is achieved.

Note that an efficient implementation of the KKR-NLCPA to the ferromagnetic alloy system $FePt$ has recently been given in [37]. In particular, [37] shows how convergence of the above algorithm can be stabilised by recasting into a form that goes back to the work of Mills [38], and details how computational effort can be reduced by making use of symmetry.

**Choice of cluster**

The restrictions on the choice of cluster in the NLCPA has been mentioned in Section 2. The construction for choosing suitable clusters and finding the cluster sites and cluster momenta satisfying (11) was first given in [15] in the context of the 2D square lattice, and generalised to realistic 3D lattices in [18–20]. Fig. 6 shows example small clusters and corresponding tiles for the commonly encountered $bcc$ and $fcc$ lattices. Significantly, since the simple cubic tiles here have the same cubic point-group symmetry as the underlying lattice, the reciprocal space integrations can be reduced to the usual $1/48^{th}$ irreducible wedge. Computationally, one can simply integrate over the irreducible parts of each tile, the total sum being the $1/48^{th}$ irreducible wedge of the original lattice. Note that KKR-NLCPA calculations have recently been carried out using $N_c = 8$ clusters in [39].

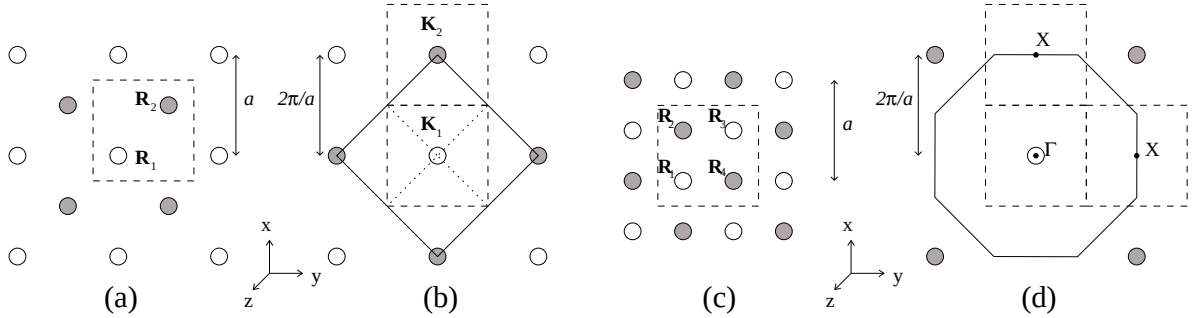


Figure 6: (a) Cross-section of a real-space tile (dashed line) for the $bcc$ lattice with $N_c = 2$ cluster containing the points $\mathbf{R}_1 = (0,0,0)$ and $\mathbf{R}_2 = (a/2, a/2, a/2)$. The shaded sites lie out of the page. (b) Cross-section of the corresponding reciprocal-space tiles (dashed lines) for the $N_c = 2$ cluster, with $\mathbf{K}_1 = (0,0,0)$ and $\mathbf{K}_2 = (2\pi/a, 0, 0)$ at their centres. The shaded points lie out of the page and the solid line denotes a cross-section of the first BZ in the $(k_x, k_y)$ plane. The BZ can be visualised as a cube with a pyramid attached to each of the six faces, and the dotted line shows a projection of such a pyramid into the $k_z$ plane. (c) Cross-section of a real-space tile (dashed line) for a $N_c = 4$ cluster on the $fcc$ lattice containing the points $\mathbf{R}_1 = (0,0,0)$, $\mathbf{R}_2 = (a/2, 0, a/2)$, $\mathbf{R}_3 = (a/2, a/2, 0)$ and $\mathbf{R}_4 = (0, a/2, a/2)$. The shaded sites lie out of the page. (d) Cross-section of the corresponding reciprocal-space tiles (dashed lines) for the $N_c = 4$ cluster, with $\mathbf{K}_1 = (0,0,0)$, $\mathbf{K}_2 = (2\pi/a, 0, 0)$, and $\mathbf{K}_3 = (0, 2\pi/a, 0)$ shown as the $\Gamma$ point and the two $X$ points. The fourth tile is centered at the $X$ point $\mathbf{K}_4 = (0, 0, 2\pi/a)$ and is situated out of the page vertically above $\Gamma$. Again the shaded points lie out of the page and the solid line denotes a cross-section of the first BZ in the $(k_x, k_y)$ plane.

**Results**

To illustrate the differences between the KKR-NLCPA and the conventional KKR-CPA as a result of nonlocal scattering correlations and chemical SRO, selected calculations are presented here for the $Cu_{50}Zn_{50}$ system using $Cu$ and $Zn$ potentials that come from self-consistent field SCF-KKR-CPA calculations. First, Fig. 7(a) shows DOS plots for pure $Cu$ and pure $Zn$, and Fig. 7(b) shows a calculation for the long-range ordered $Cu_{50}Zn_{50}$ inter-metallic compound (which exists below the transition temperature). Since the energies of the $Cu$ and $Zn$ $d$-bands are very different, the system is said to be in the 'split band' regime. Physically, this means an electron travels more easily between like sites than between unlike sites and so this results in a narrowing of the $Cu$ and $Zn$ bands by a factor of two in the ordered calculation compared with the pure calculations [40]. Fig. 7(c) shows KKR-CPA results for disordered $bcc$ $Cu_{50}Zn_{50}$. It is clear that the bands are widened and smoothened compared with the DOS for the ordered calculation. The component contributions from $Cu$ and $Zn$ impurity sites embedded in the KKR-CPA medium are also shown. Next, a KKR-NLCPA calculation for disordered $Cu_{50}Zn_{50}$ for a two-site cluster ($N_c = 2$) is shown in Fig. 7(d). First note that there is little observable difference in the total DOS compared with the KKR-CPA calculation. This is due to the small size of the cluster so that the difference due to the nonlocal scattering correlations shows up in detail only on a scale of $\pm 1$ state/atom/Ry (see Ref. [20]). However the most striking aspect of the KKR-NLCPA calculation is that the component contributions to the total DOS from the four possible cluster configurations are apparent. The component plots here are the DOS measured at the first cluster site when a particular cluster configuration is embedded in the KKR-NLCPA medium, which is the $Cu$ site for the $Cu$-$Cu$ and

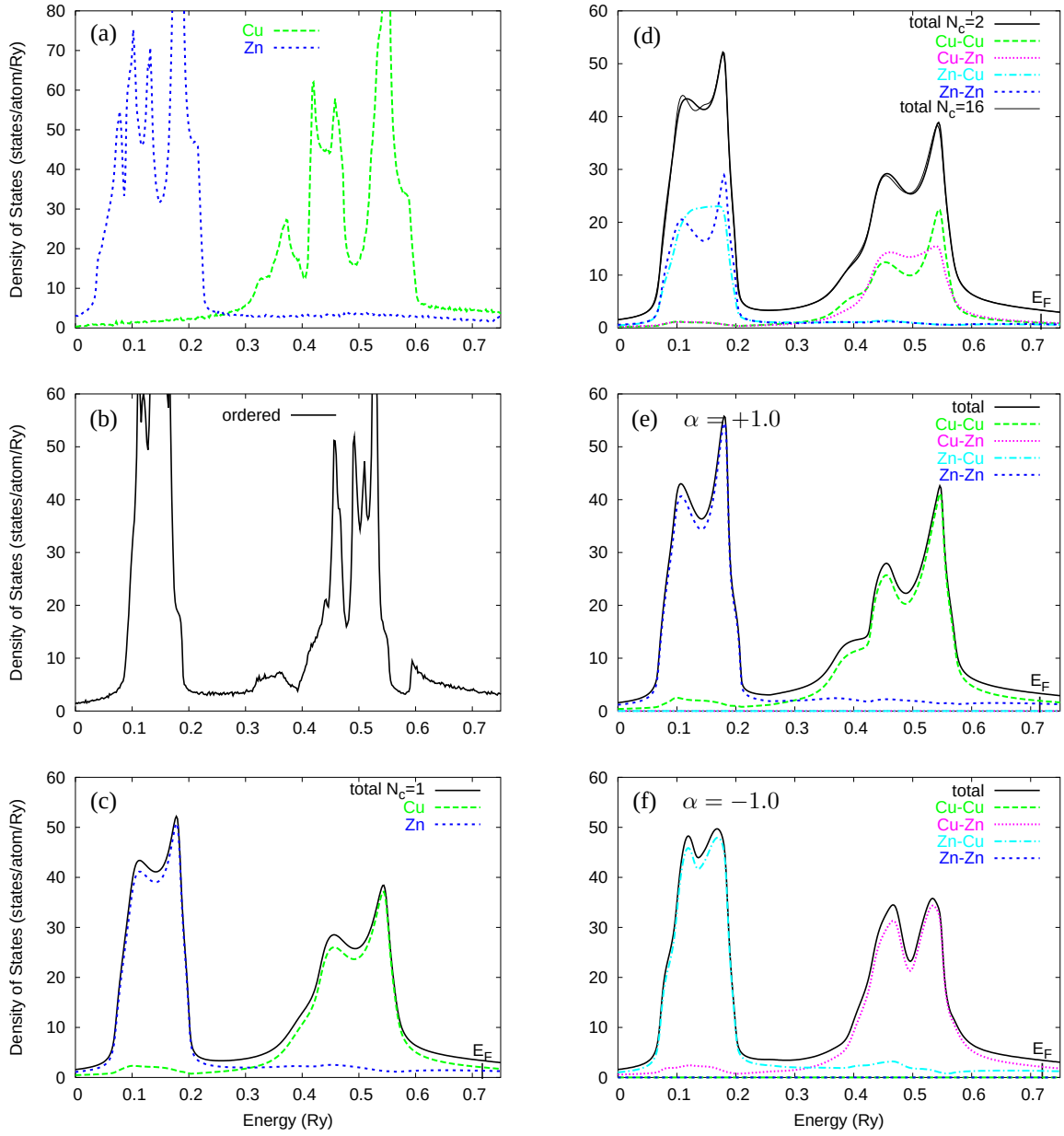


Figure 7: (a) Density of states (DOS) for pure $Cu$ and pure $Zn$. (b) DOS for ordered $Cu_{50}Zn_{50}$. (c) Total average DOS for disordered *bcc* $Cu_{50}Zn_{50}$ using the KKR-CPA. Also shown are the contributions from the $Cu$ and $Zn$ components (single-site partially-averaged DOS). $E_F$ is the Fermi energy. (d) Total average DOS for *bcc* $Cu_{50}Zn_{50}$ using the KKR-NLCPA with $N_c = 2$, along with the contributions from the 4 possible cluster configurations (cluster partially-averaged DOS) measured at the first site i.e. $Cu$ for $Cu$-$Cu$, $Cu$-$Zn$, and $Zn$ for $Zn$-$Cu$, $Zn$-$Zn$. (Owing to the translational invariance, contributions measured at the second site would give the same results with a simple reversal of the labels). Also shown are total DOS results for $N_c = 16$. (e) Same as (d) but with SRO parameter $\alpha$=+1.0, corresponding to ideal short-range clustering. (f) Same as (d) but with SRO parameter $\alpha$=-1.0, corresponding to ideal short-range ordering.

$Cu$-$Zn$ configurations, and the $Zn$ site for the $Zn$-$Cu$ and $Zn$-$Zn$ configurations. Crucially, owing to the translational invariance of the KKR-NLCPA medium, measurement at the second site gives the same results with a simple reversal of the labels of the $Cu$-$Zn$ and $Zn$-$Cu$ components. These component plots are particularly useful for interpreting the effects of SRO on the electronic structure. For a cluster of size $N_c = 2$, it is possible to include SRO between nearest neighbour sites only. This may be straightforwardly done by introducing the nearest neighbour Warren-Cowley SRO parameter $\alpha$ [41], and using probabilities defined as $P_{CuCu} = P_{Cu}^2 + \alpha/4$, $P_{ZnZn} = P_{Zn}^2 + \alpha/4$, $P_{CuZn} = P_{Cu}P_{Zn} - \alpha/4$, and $P_{ZnCu} = P_{Zn}P_{Cu} - \alpha/4$. For $Cu_{50}Zn_{50}$, $P_{Cu} = P_{Zn} = 0.5$ and so possible values in the range $-1 \leq \alpha \leq 1$, where $-1$, 0 and $+1$ correspond to ideal ordering, complete randomness, and ideal clustering. For example, at $\alpha = +1$ the probability of unlike pairs is zero and the total DOS is now completely dominated by the features of the $Cu$-$Cu$ and $Zn$-$Zn$ components, as shown in Fig. 7(e). As expected these features are reminiscent of the pure bands shown in Fig. 7(a). At the other extreme case $\alpha = -1$, as shown in Fig. 7(f), there are only contributions remaining from unlike pairs and the DOS in general has a closer resemblance to that of ordered $Cu_{50}Zn_{50}$ shown in Fig. 7(b).

# 4 Self-Consistent-Field (SCF)-KKR-NLCPA

The calculations presented in Section 3 were 'first-pass' KKR-NLCPA calculations only i.e. the potentials used were self-consistently determined using the conventional SCF-KKR-CPA, and then a single KKR-NLCPA calculation performed using these potentials. In other words, although the potentials were charge self-consistent with respect to the KKR-CPA medium, they were not charge self-consistent with respect to the new KKR-NLCPA medium. In order to appreciate the new physics that could be described by a charge self-consistent (SCF)-KKR-NLCPA [21], first recall that a disordered alloy as a whole is charge neutral. This implies that the effective medium representing the exact configurational average over all disorder configurations described by (42) shares this property. Moreover, since the medium is translationally-invariant, this implies that each site in the effective medium must be charge neutral. The problem with the conventional SCF-KKR-CPA method is that in setting up this medium, a single $A$ or $B$ impurity site embedded in the medium can only interact with this neutral environment i.e. the exchange of charge with other $A$ and $B$ sites belonging to specific disorder configurations is not taken into account. This in turn means there is an intersite Madelung electrostatic contribution missing in the SCF-KKR-CPA total energy expression for the alloy.

In order to see how to go beyond the SCF-KKR-CPA description of charges, it is important to realise that in a real alloy, say $Cu_{50}Zn_{50}$, we no longer only have one $Cu$ and one $Zn$ potential. This is because for any given disorder configuration, each $Cu$ site and each $Zn$ site will have a different environment i.e. differing numbers of $Cu$ and $Zn$ neighbours. This means that when charge redistributes itself to minimise the total energy for that configuration, there will in principle be a different potential on every site in the lattice [42]. In order to bridge the gap between the SCF-KKR-CPA and the exact result (within LDA), a charge self-consistent SCF-KKR-NLCPA must therefore go beyond a two-potential description of a binary alloy. The SCF-KKR-NLCPA achieves this by enforcing self-consistency with respect to a set of $N_c \times 2^{N_c}$ *cluster potentials* $\underline{v}_\gamma$ which depend on a set of partially-averaged *cluster charge densities* $\underline{\rho}_\gamma$. Due to the Born-von Karman boundary conditions imposed on the cluster, the charge self-consistent medium will be translationally-invariant and therefore each site will be charge neutral.

However, in setting up the medium, charge is allowed to transfer between the cluster sites and hence we will systematically gain an intersite Madelung electrostatic contribution to the total energy which was missing in the SCF-KKR-CPA.

In the interest of clarity it is useful to introduce the following notation. By measuring the partially-averaged (i.e. component) cluster charge density via (53) at each site in the cluster for the fixed configuration $\gamma$, we may define the cluster component charge density matrix $\underline{\rho}_\gamma(\mathbf{r})$ such that

$$\left[\underline{\rho}_\gamma(\mathbf{r})\right]_{II} = \rho_\gamma(\mathbf{r}_I)$$

where $\mathbf{r}_I$ implies that $\mathbf{r}$ restricted to lie within site $I$, and is measured from the nuclear position $\mathbf{R}_I$. Similarly, we introduce the cluster potential matrix $\underline{v}_\gamma(\mathbf{r})$ with site matrix elements

$$\left[\underline{v}_\gamma(\mathbf{r})\right]_{II} = v_\gamma(\mathbf{r}_I).$$

As an example, for the simple case of a two-site cluster for a binary alloy we will have $2^2 = 4$ cluster potential and cluster component charge density matrices, and will have $2^2 \times 2 = 8$ distinct single-site potentials (which can be reduced to 4 using symmetry e.g. $v_{AA}(\mathbf{r}_I) = v_{AA}(\mathbf{r}_J)$, $v_{AB}(\mathbf{r}_I) = v_{BA}(\mathbf{r}_J)$ etc.). For the configuration $\gamma = \{AB\}$ we have

$$\underline{v}_\gamma(\mathbf{r}) = \begin{bmatrix} v_{AB}(\mathbf{r}_I) & 0 \\ 0 & v_{AB}(\mathbf{r}_J) \end{bmatrix} \quad \text{and} \quad \underline{\rho}_\gamma(\mathbf{r}) = \begin{bmatrix} \rho_{AB}(\mathbf{r}_I) & 0 \\ 0 & \rho_{AB}(\mathbf{r}_J) \end{bmatrix}$$

Although the potentials are single-site quantities, it is still necessary to include the full configuration label. This is because although for example $v_{AB}(\mathbf{r}_J)$ is a '$B$' site, $v_{AB}(\mathbf{r}_J)$ is not the same single-site potential as $v_{BB}(\mathbf{r}_J)$. The same notation must also be applied to the corresponding wavefunctions and cluster $t$-matrices when attempting to obtain self-consistent potentials e.g. for the configuration $\gamma = \{AB\}$ we have

$$\underline{\underline{Z}}_\gamma = \begin{bmatrix} \underline{Z}_{AB}(\mathbf{r}_I, E) & 0 \\ 0 & \underline{Z}_{AB}(\mathbf{r}_J, E) \end{bmatrix} \quad \text{and} \quad \underline{\underline{t}}_{cl,\gamma} = \begin{bmatrix} \underline{t}^I_{AB} & \underline{G}(\mathbf{R}_{IJ}) \\ \underline{G}(\mathbf{R}_{JI}) & \underline{t}^J_{AB} \end{bmatrix}$$

**Total energy**

By integrating Maxwell's relation $N = -(\partial\Omega/\partial\mu)$ for a fixed configuration where $N$ is the number of electrons, it can be shown that the fundamental equation for the configurationally-averaged electronic grand potential is given by [10, 11]

$$\overline{\Omega} = \mu\overline{N}(\mu,\mu) - \int_{-\infty}^{\mu} dE\, \overline{N}(E,\mu) + \int_{-\infty}^{\mu} d\mu' \int_{-\infty}^{\mu'} dE\, \frac{\delta\overline{N}(E,\mu')}{\delta\mu'} \tag{54}$$

where $\overline{N}$ is the configurationally-averaged integrated density of states per site at constant temperature and volume, and $\mu$ is the electronic chemical potential. Adding the energy of the ion-ion interactions to $\overline{\Omega}$ gives the total internal energy of the system. The significance of the above equation is that only an approximation for $\overline{N}$ is required, together with its variation with respect to $\mu$. Within the KKR-NLCPA, it can be straightforwardly shown that $\overline{N}$ is given by the Lloyd formula

$$\begin{aligned} \overline{N}(E,\mu) &= N_o(E) - \frac{1}{\pi}\frac{1}{\Omega_{BZ}} Im\left[\sum_{\mathbf{K}_n}\int_{\Omega_{\mathbf{K}_n}} d\mathbf{k}\ ln\|\widehat{\underline{t}}^{-1} - \widehat{\underline{\delta G}}(\mathbf{K}_n) - \underline{G}(\mathbf{k})\|\right] \\ &- \frac{1}{\pi N_c} Im\left[\sum_\gamma P_\gamma ln\|\underline{\tau}_\gamma^{-1}\| - ln\|\widehat{\underline{\tau}}^{-1}\|\right] \end{aligned} \tag{55}$$

where $N_o$ is the free-electron contribution and all other terms have been defined in Section 3. The determinants in the final term are over both the angular momentum and cluster-site indices. By evaluating $d\overline{N}/d\mu$, substituting into (54), and then performing the integration with respect to $\mu'$ by parts [21], an expression for the electronic grand potential in terms of the cluster potentials and cluster charge densities is obtained in the form

$$\begin{aligned}\overline{\Omega} &= \mu\overline{N}(\mu,\mu) - \int_{-\infty}^{\mu} dE\,\overline{N}(E,\mu) - \frac{1}{N_c}\sum_{\gamma} P_\gamma \sum_I \left( \int d\mathbf{r}_I \rho_\gamma(\mathbf{r}_I,\mu)\, v_\gamma(\mathbf{r}_I,\mu) \right) \\ &+ \frac{1}{N_c}\int_{-\infty}^{\mu} d\mu' \sum_{\gamma} P_\gamma \sum_I \left( \int d\mathbf{r}_I\, v_\gamma(\mathbf{r}_I,\mu') \frac{d\rho_\gamma(\mathbf{r}_I,\mu')}{d\mu'} \right) \end{aligned} \tag{56}$$

We now need a specific form for the cluster potential $\underline{v}_\gamma(\mathbf{r})$. As a generalisation of the SCF-KKR-CPA approach described in Section 3, we choose $\underline{v}_\gamma(\mathbf{r})$ to depend on the partially-averaged cluster charge densities $\underline{\rho}_\gamma(\mathbf{r})$ within the cluster and on the average charge density outside. So for a particular cluster configuration $\gamma$, we choose $\underline{v}_\gamma(\mathbf{r})$ within a cluster site $I$ to take the form

$$\begin{aligned} v_\gamma(\mathbf{r}_I) &= \sum_J \int d\mathbf{r}'_J \frac{\rho_\gamma(\mathbf{r}'_J)}{|\mathbf{r}_I - \mathbf{r}'_J + \mathbf{R}_{IJ}|} - \sum_J \frac{Z_\gamma^J}{|\mathbf{r}_I + \mathbf{R}_{IJ}|} \\ &+ \sum_{n\notin C} \int d\mathbf{r}'_n \frac{\overline{\rho}(\mathbf{r}'_n)}{|\mathbf{r}_I - \mathbf{r}'_n + \mathbf{R}_{In}|} - \sum_{n\notin C} \frac{\overline{Z}^n}{|\mathbf{r}_I + \mathbf{R}_{In}|} + v_\gamma^{xc}\left[\rho_\gamma(\mathbf{r}_I)\right] \end{aligned} \tag{57}$$

where the sums in the first line are over all sites $J$ (including $J = I$) belonging to the cluster, and the sums in the second line are over all sites $n$ outside of the cluster. Notation has been introduced such that the nuclear charge on a cluster site $I$ for the fixed cluster configuration $\gamma$ is labeled as $Z_\gamma^I$. So the first and second terms in (57) represent the electronic and nuclear Coulomb contributions respectively at $\mathbf{r}_I$ from each site in the cluster for the fixed configuration $\gamma$. The average charge and nuclear densities placed on all sites outside the cluster are given by $\overline{\rho}(\mathbf{r}_n) = \sum_\gamma P_\gamma \rho_\gamma(\mathbf{r}_I)$ and $\overline{Z}^n = \sum_\gamma P_\gamma Z_\gamma^I$ respectively (note any cluster site $I$ may be chosen to calculate these since all sites are equivalent after averaging over all cluster configurations, a consequence of the Born-von Karman boundary conditions imposed on the cluster). Since each site is neutral on the average (but *not independently from the other sites* as in the KKR-CPA), we have $\int d\mathbf{r}_n\, \overline{\rho}(\mathbf{r}_n) - \overline{Z}^n = 0$. However these contributions from outside the cluster should still be included as there is in general a multipole contribution arising from them (e.g. for a non-spherical charge distribution). The final term in (57) represents the exchange correlation potential [6, 7] at $\mathbf{r}_I$, given that the impurity cluster configuration is $\gamma$. Now inserting (57) into the final term of (56) and performing the integration with respect to $\mu'$ by parts [21] leads to the expression for the electronic grand potential in the form

$$\begin{aligned}\overline{\Omega} &= \mu\overline{N}(\mu,\mu) - \int_{-\infty}^{\mu} dE\,\overline{N}(E,\mu) - \frac{1}{N_c}\sum_{\gamma} P_\gamma \sum_I \int d\mathbf{r}_I\, \rho_\gamma(\mathbf{r}_I,\mu)\, v_\gamma(\mathbf{r}_I,\mu) \\ &+ \frac{1}{2}\frac{1}{N_c}\sum_{\gamma} P_\gamma \sum_I \sum_J \frac{\int d\mathbf{r}_I\, \rho_\gamma(\mathbf{r}_I)\left(\int d\mathbf{r}'_J\, \rho_\gamma(\mathbf{r}'_J) - 2Z_\gamma^J\right)}{|\mathbf{r}_I - \mathbf{r}'_J + \mathbf{R}_{IJ}|} \\ &+ \frac{1}{2}\frac{1}{N_c}\sum_{\gamma} P_\gamma \sum_I \sum_{n\notin C} \frac{\int d\mathbf{r}_I\, \rho_\gamma(\mathbf{r}_I)\left(\int d\mathbf{r}'_n\, \overline{\rho}(\mathbf{r}'_n) - 2\overline{Z}^n\right)}{|\mathbf{r}_I - \mathbf{r}'_n + \mathbf{R}_{In}|} \\ &+ \frac{1}{N_c}\sum_{\gamma} P_\gamma \sum_I \int d\mathbf{r}_I\, \rho_\gamma(\mathbf{r}_I) v_\gamma^{xc}\left[\rho_\gamma(\mathbf{r}_I)\right] \end{aligned} \tag{58}$$

In the above expression the first line represents the configurationally-averaged kinetic energy. The second line involves Coulomb interactions between all cluster sites for each fixed impurity configuration $\gamma$. This is because charge is allowed to transfer between the cluster sites and so there will be a net (and different) overall charge on each cluster site. After the average over all configurations $\gamma$ is taken, charge neutrality per site will be restored, however we have gained the energy contribution given in the second line. The off-diagonal part of this term (i.e. when $J \neq I$) represents charge correlations between the cluster sites, such terms being absent in the conventional single-site KKR-CPA expression. An estimate of the Madelung contribution to the total energy per site missing in the single-site KKR-CPA may therefore be calculated by excluding the $J = I$ terms from the summation, yielding

$$E_{Madelung} = \frac{1}{2}\frac{1}{N_c}\sum_{\gamma} P_{\gamma} \sum_{I}\sum_{J\neq I} \frac{\int d\mathbf{r}_I \, \rho_{\gamma}(\mathbf{r}_I)\left(\int d\mathbf{r}'_J \, \rho_{\gamma}(\mathbf{r}'_J) - 2Z_{\gamma}^{J}\right)}{|\mathbf{r}_I - \mathbf{r}'_J + \mathbf{R}_{IJ}|} \tag{59}$$

for a cluster of size $N_c$. The third line of (58) represents the contributions from the average electronic and nuclear charges outside the cluster. The final term (fourth line) is the exchange-correlation energy. Finally, note that due to translational invariance, (58) and (59) may be simplified for computational purposes by removing the $1/N_c$ factor and the sum over cluster sites $I$, although the sum over $J$ remains.

**Charge self-consistency**

Recall that in DFT for usual systems the total energy or $\Omega$ is stationary with respect to the ground-state charge density with the condition that the number of particles $N$ is kept constant. The total energy within the conventional KKR-CPA maintains this variational property since $\Omega$ is stationary with respect to the partially-averaged charge densities $\rho_{\alpha}(\mathbf{r})$, where $\alpha$ is the atomic species i.e. $\delta\{\Omega - \mu\overline{N}\}/\delta\rho_{\alpha}(\mathbf{r}) = 0$ [11]. Significantly, as a generalisation of this it can be shown that the total energy expression within the KKR-NLCPA above is also variational i.e. $\delta\{\Omega - \mu\overline{N}\}/\delta(\rho_{\gamma}(\mathbf{r}_I)) = 0$ for each cluster configuration $\gamma$ where $\mathbf{r}_I$ is a point within any cluster site $I$ [21]. This variational property arises from the combined effects of the variational properties of DFT and the KKR-NLCPA, and establishes the charge self-consistency procedure which is briefly outlined below.

- Begin with an appropriate guess for the set of $2^{N_c}$ cluster potential matrices $\underline{v}_{\gamma}(\mathbf{r})$.
- Calculate the corresponding cluster t-matrices and use the KKR-NLCPA to determine the effective medium.
- Calculate the site-diagonal part of the partially-averaged cluster Green's functions $\underline{\underline{G}}_{\gamma}(\mathbf{r},\mathbf{r})$ and from these calculate the corresponding partially-averaged cluster charge densities $\underline{\rho}_{\gamma}(\mathbf{r})$.
- Using the charge densities above, reconstruct new cluster potentials $\underline{v}_{\gamma}(\mathbf{r})$. For a particular configuration $\gamma$, this is given by (57) for $\mathbf{r}$ lying within site $I$. This needs to be calculated for each $I$ with $I = 1, .., N_c$ for the configuration $\gamma$.
- Compare with the previous cluster potentials and iterate to self-consistency.

**Results**

In order to explicitly demonstrate the differences between the new SCF-KKR-NLCPA calculations compared to the non-SCF KKR-NLCPA calculations given in Section 3, the same $bcc\ Cu_{50}Zn_{50}$ system is

studied here. Fig. 8(b) shows a new SCF-KKR-NLCPA calculation for the DOS with $N_c = 2$ and no SRO (i.e. $\alpha = 0$ as defined in Section 3), together with the conventional SCF-KKR-CPA result. Again, the contributions from the four possible cluster configurations are also shown. It is clear that there is now an observable difference between the total DOS results using the new SCF-KKR-NLCPA compared to the SCF-KKR-CPA. This difference is plotted in Fig. 8(c), and integrates to zero since there are the same number of electrons (11.5) per site in both cases (the Fermi level has been subtracted separately for each total DOS plot in Fig. 8). As can be seen by comparing the corresponding component DOS plots with the non-SCF KKR-NLCPA results shown in Fig. 8(a), this difference arises from charge transfer between the cluster sites at certain energy regions. Here the energy regions in which this occurs are well separated since $Cu_{50}Zn_{50}$ is in the 'split band' regime.

Now let us consider the total energy of the system. Fig. 8(d) shows that there is an overall lowering of the total energy (of order 0.28 mRy) calculated using the SCF-KKR-NLCPA for $\alpha = 0$ compared with the SCF-KKR-CPA calculation. The Madelung contribution to the total energy calculated via (59) is -2.41 mRy. This compares favourably with values of -2.5 mRy and -2.67 mRy previously obtained using large supercell calculations in Refs. [43] and [44] respectively. Significantly, it is found that the difference in the total energy is much smaller than the magnitude of the Madelung contribution because changes in the potential contribution are largely compensated for by corresponding changes in the kinetic contribution when the Madelung term is included in such self-consistent calculations.

Finally let us consider the effects of SRO on the total energy of the system [45]. The physics of SRO plays a particularly important role near phase transitions where it is frequently a precursor for long range order and can be said to be driving the ordering process. In the ordering of the $Cu_{50}Zn_{50}$ solid solution into an intermetallic compound of $B2$ symmetry the system lowers its free energy by having unlike neighbours more frequently than like neighbours even in the disordered state, thereby lowering the temperature $T_c$ where the system must finally order. We would therefore expect the total energy calculated using the SCF-KKR-NLCPA to be lower for negative values of $\alpha$, corresponding to short-range ordering. Fig. 8(d) shows SCF-KKR-NLCPA calculations with $N_c = 2$ for the total energy plotted as a function of SRO (the corresponding DOS plots can be found in Ref. [21]). Reassuringly, it can be seen that the total energy is indeed lowered as $\alpha$ decreases. Furthermore the relationship between the total energy and SRO parameter is found in this case to be linear. However, it should be stressed that the SCF-KKR-NLCPA is a theory of the electronic structure for a given ensemble of alloy configurations and is not a theory for what configurations actually occur in practice. For example, the extreme case corresponding to $\alpha = -1.0$ (as defined in Section 3) means that only unlike pairs are included in the $N_c = 2$ cluster ensemble, a situation which would not occur in a real disordered alloy. The actual favoured amount of SRO at a given temperature above $T_c$ would need to be found by minimising the corresponding free energy with respect to the SRO parameter $\alpha$. This requires an expression for the configurational entropy term for the cluster with SRO, and would amount to a first-principles cluster variational method [46]. Work is currently being carried out on this development.

## 5 Conclusions and future work

A review of the nonlocal coherent-potential approximation (NLCPA) has been presented, both within the tight-binding framework and within first-principles multiple scattering theory (KKR-NLCPA). The

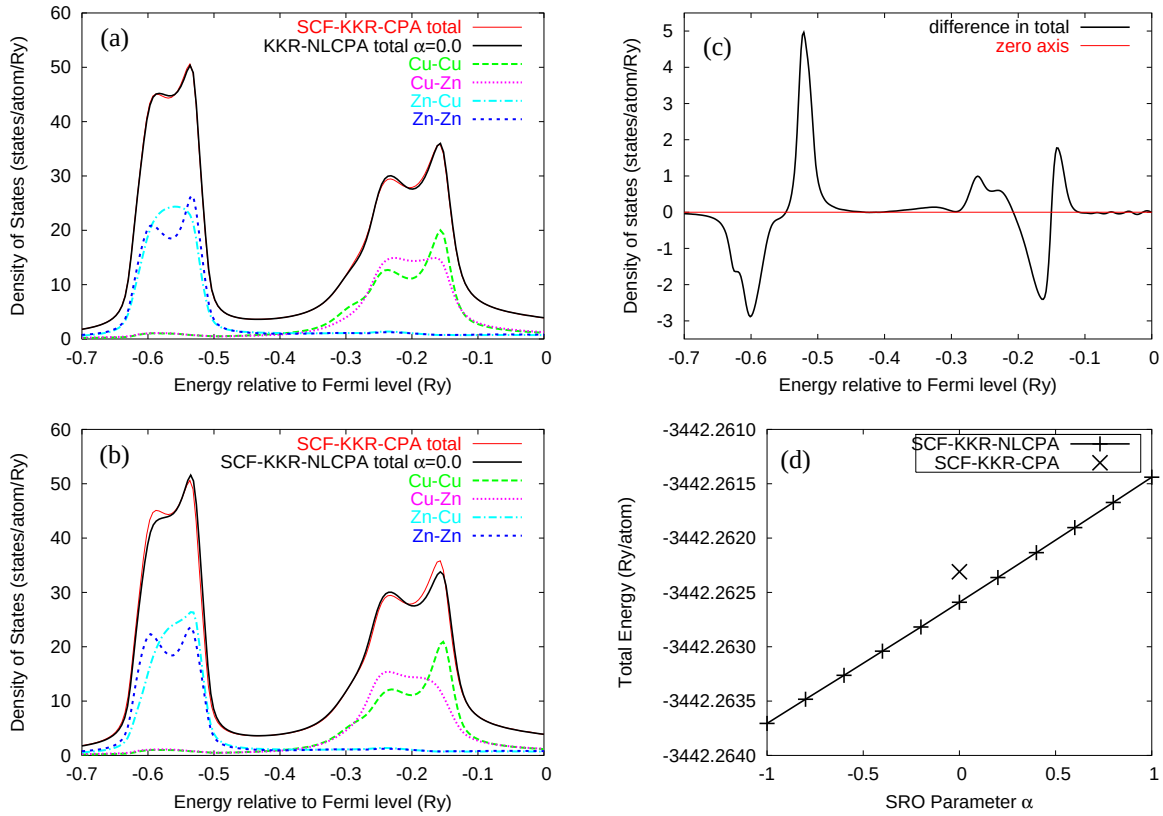


Figure 8: (Data obtained by A. Ernst) (a) Total average DOS for disordered $bcc\ Cu_{50}Zn_{50}$ using the (non-SCF) KKR-NLCPA with $N_c = 2$ and $\alpha = 0$. Also shown are the contributions from the four possible cluster configurations (measured at the first labelled site). The total conventional SCF-KKR-CPA result is also shown for comparison. (b) Same as above but using the new self-consistent-field (SCF)-KKR-NLCPA. Notice the differences in the cluster component contributions compared to (a) as a result of charge transfer. (c) Plot of the difference between the total SCF-KKR-CPA and total SCF-KKR-NLCPA results shown in (b) due to charge transfer. (d) Total energy for disordered $bcc\ Cu_{50}Zn_{50}$ using the SCF-KKR-NLCPA with $N_c = 2$ as a function of SRO parameter $\alpha$. Also shown is the conventional SCF-KKR-CPA result (at $\alpha = 0$).

NLCPA generalises the conventional CPA approach to dealing with disordered systems by systematically enabling important short-range environmental effects present in the individual disorder configurations to be included in its configurationally-averaged description of the system. A fully charge self-consistent version of the theory (SCF-KKR-NLCPA) has been demonstrated by investigating the effects of charge-correlations and chemical short-range order on the $Cu_{50}Zn_{50}$ solid solution.

In regard to the computational issues of the method itself, the SCF-KKR-NLCPA has relatively low computational cost in comparison with supercell-based methods since the Brillouin zone integration does not scale as the cluster size increases. The only computational cost compared to the conventional SCF-KKR-CPA is due to averaging over the $2^{N_c}$ real-space cluster configurations, where $N_c$ is the number of sites in the cluster. For calculations with small cluster sizes such as $N_c = 2$ and $N_c = 4$, there is therefore very little increase in computational cost over the conventional SCF-KKR-CPA method. Moreover, calculations with such cluster sizes are, for example, able to model the effects of nearest-neighbour SRO and are able to capture a large fraction of the Madelung energy in alloys. However, calculations for larger cluster sizes will be computationally very demanding and it will clearly be necessary to use importance sampling to greatly reduce the number of configurations. Furthermore, calculations for a simple 1D tight-binding model show that for cluster sizes below a critical value $N_{critical}$, results obtained using both periodic and anti-periodic Born-von Karman boundary conditions applied to the cluster should be combined. This can be straightforwardly carried out using the method proposed in Ref. [34], and has the advantage of yielding a spectral function with no discontinuities (thus facilitating its application to SRO studies of transport properties and Fermi surfaces). A systematic study of the convergence of the KKR-NLCPA with respect to cluster size is currently being carried out to establish the value of $N_{critical}$ for various realistic systems.

Finally, recall that the conventional SCF-KKR-CPA has been used as an electronic basis for a first-principles mean-field theory of the configurational statistical mechanics of the concentration fluctuations in alloys [47, 48]. In terms of future alloy-based work based on the SCF-KKR-NLCPA, it is clear that the cluster probabilities $\{P_\gamma\}$ used to calculate the total energy or electronic grand potential specify the corresponding cluster configurational entropy. These probabilities, which include a specification of SRO, may therefore be determined by constructing the appropriate free energy and minimizing it with respect to them (strain fluctuations [49] i.e. lattice displacements, could similarly be treated). This would amount to a fully first-principles cluster variational method [46] which can be expected to yield reliable alloy phase diagrams. Moreover, the SCF-KKR-CPA has also been adapted to treat valency fluctuations in pseudo-alloys [26], and adapted to deal with the disordered local moment (DLM) spin fluctuations in itinerant magnets at finite temperature [12, 13]. The SCF-KKR-NLCPA could similarly be adapted to investigate the creation of $\gamma$-like $Ce$ atoms near the $\gamma - \alpha$ transition in a pseudo-alloy treatment of $Ce$, and to include correlations in the orientations of the local moments to facilitate the formation of the DLM state of $Ni$-rich systems.

## Acknowledgments

Thanks to G. M. Batt, A. Ernst, B. L. Györffy and J. B. Staunton for collaborating on parts of the work reviewed in this highlight. This work was funded by EPSRC (U.K.).

## References


[1] P. Soven, Phys. Rev. **156**, 809 (1967).

[2] J. Korringa, Physica **13**, 392 (1947).

[3] W. Kohn and N. Rostoker, Phys. Rev. **94**, 1111 (1954).

[4] B. L. Györffy, Phys. Rev. B **5**, 2382 (1972).

[5] G. M. Stocks, W. M. Temmerman, and B. L. Györffy, Phys. Rev. Lett. **41**, 339 (1978).

[6] P. Hohenberg and W. Kohn, Phys. Rev. **136**, B864 (1964).

[7] W. Kohn and L. J. Sham, Phys. Rev. **140**, A1133 (1965).

[8] G. M. Stocks and H. Winter, Z. Phys. B **46**, 95 (1982).

[9] H. Winter and G. M. Stocks, Phys. Rev. B. **27**, 882 (1983).

[10] D. D. Johnson *et al.*, Phys. Rev. Lett. **56**, 2088 (1986).

[11] D. D. Johnson *et al.*, Phys. Rev. B. **41**, 9701 (1990).

[12] B. L. Györffy *et al.*, J. Phys. F: Met. Phys. **15**, 1337 (1985).

[13] J. B. Staunton and B. L. Györffy, Phys. Rev. Lett. **69**, 371 (1992).

[14] A. Gonis, *Green Functions for Ordered and Disordered Systems*, Vol. 4 of *Studies in Mathematical Physics* (North Holland, Amsterdam, 1992).

[15] M. Jarrell and H. R. Krishnamurthy, Phys. Rev. B **63**, 125102 (2001).

[16] M. H. Hettler *et al.*, Phys. Rev B. **58**, 7475 (1998).

[17] M. H. Hettler, M. Mukherjee, M. Jarrell, and H. R. Krishnamurthy, Phys. Rev. B **61**, 12739 (2000).

[18] D. A. Rowlands, *'The KKR-NLCPA: a new method for describing the electronic structure of disordered metallic sytems'*, Ph.D. Thesis, University of Warwick (2004).

[19] D. A. Rowlands, J. B. Staunton, and B. L. Györffy, Phys. Rev. B. **67**, 115109 (2003).

[20] D. A. Rowlands, J. B. Staunton, B. L. Györffy, E. Bruno and B. Ginatempo, cond-mat/0411347, Phys. Rev. B **72**, 045101 (2005).

[21] D. A. Rowlands, A. Ernst, B. L. Györffy, and J. B. Staunton, Phys. Rev. B. **73**, 165122 (2006).

[22] R. Magri, S.-H. Wei, and A. Zunger, Phys. Rev. B **42**, 11388 (1990).

[23] L. W. Lu, S.-H. Wei, and A. Zunger, Phys. Rev. Lett. **66**, 1753 (1991).

[24] A. Zunger, in *Structural and Phase Stability of Alloys*, edited by J. L. Moran-Lopez, F. Mejia-Lira, and J. M. Sanchez (Plenum, New York, 1992), Chap. 17.

[25] A. Zunger, in *Statics and Dynamics of Alloy Phase Transformations*, Vol. 319 of *NATO Advanced Study Institute Series B: Physics*, edited by A. Gonis and P. E. A. Turchi (Plenum, New York, 1993).

[26] M. Lüders *et al.*, Phys. Rev. B **71**, 205109 (2005).

[27] I. Wilkinson *et al.*, Phys. Rev. Lett. **87**, 216401 (2001).

[28] R. H. Brown, P. B. Allen, D. M. Nicholson, and W. H. Butler, Phys. Rev. Lett. **62**, 661 (1989).

[29] D. F. Elliot and K. R. Rao, *Fast Transforms: Algorithms, Analyses, Applications* (Academic, New York, 1982).

[30] D. A. Rowlands, J. Phys.: Condens. Matter **18**, 3179 (2006).

[31] P. Dean, Rev. Mod. Phys. **44**, 127 (1972).

[32] M. Tsukada, J. Phys. Soc. Jpn **32**, 1475 (1972).

[33] F. Ducastelle, J. Phys. C **7**, 1795 (1974).

[34] G. M. Batt and D. A. Rowlands, submitted to J. Phys.: Condens. Matter (2006).

[35] P. R. Tulip *et al.*, Phys. Rev. B **73**, 205109 (2006).

[36] J. S. Faulkner and G. M. Stocks, Phys. Rev. B **21**, 3222 (1980).

[37] D. Ködderitzsch, H. Ebert, D. A. Rowlands and A. Ernst, submitted to Phys. Rev. B (2006).

[38] R. Mills, L. J. Gray, and T. Kaplan, Phys. Rev. B **27**, 3252 (1983).

[39] D. A. Biava *et al.*, Phys. Rev. B. **72**, 113105 (2005).

[40] V. L. Moruzzi, A. R. Williams, J. F. Janak, and C. Sofes, Phys. Rev. B. **9**, 3316 (1974).

[41] J. M. Cowley, J. Appl. Phys. **21**, 24 (1950).

[42] B. Ujfalussy *et al.*, Phys. Rev. B **61**, 12005 (2000).

[43] J. S. Faulkner, Y. Wang, and G. M. Stocks, Phys. Rev. B **55**, 7492 (1997).

[44] C. Wolverton, A. Zunger, S. Froyen, and S. H. Wei, Phys. Rev. B. **54**, 7843 (1996).

[45] I. A. Abrikosov *et al.*, Phys. Rev. Lett. **76**, 4203 (1996).

[46] J. L. Moran-Lopez and J. M. Sanchez, *Theory and Applications of the Cluster Variation and Path Probability Methods* (Plenum Press, New York, 1996).

[47] B. L. Györffy and G. M. Stocks, Phys. Rev. Lett. **50**, 374 (1983).

[48] B. L. Györffy *et al.*, in *Proc. of the NATO Advanced Study Institute on Alloy Phase Stability*, edited by G. M. Stocks and A. Gonis (Kluwer, Dordrecht, 1987), p. 421.

[49] B. L. Györffy, Physica Scripta **T49**, 373 (1993).